

Exciton-phonon interaction in planar nitride nanostructures: The case of acoustic phononsIgor Boyko ^{*}*Ternopil Ivan Puluj National Technical University, Ternopil 46001, Ukraine*

(Received 16 March 2023; revised 19 June 2023; accepted 24 July 2023; published 7 August 2023)

A quantum mechanical theory which describes the exciton-acoustic phonon interaction in plane semiconductor AlN/AlGaN nanosystems at nonzero temperatures has been developed. The theory of exciton states is constructed by applying the effective mass model to an electron and a hole, taking into account internal electric fields due to the macroscopic value of polarization, which is a significant factor affecting the states of quasiparticles in nitride nanosystems. The theory of acoustic phonons was developed on the basis of the elastic continuum model by analytically obtained solutions of the equations describing the components of the deformation field of a semiconductor medium. We have considered both relevant cases, when the semiconductors forming the studied nanosystem have a wurtzite-type crystal lattice and a zinc-blende-type lattice. In addition, we obtained analytical expressions that specify the deformation and piezoelectric potential created by acoustic phonons for these cases. For each type of crystal lattice, the cases of exciton-phonon interaction through the deformation and piezoelectric potentials have been separately and sufficiently investigated. The theory of exciton-phonon interaction was developed and characteristics of the renormalized exciton states were investigated using the method of temperature Green's functions using and the Dyson equation. We found that for wurtzite nanosystems, the mechanisms of interaction through the piezoelectric and deformation potentials contribute to the exciton-phonon interaction, while for zinc-blende nanosystems, the main contribution to this interaction is due to the deformation potential. It is found that the temperature shifts of the exciton spectrum are of negative sign for all temperatures, and the absolute values of these shifts increase with the temperature increase. An analysis of the calculated exciton basic band shape function and decay rates made it possible to establish that, in the case of the zinc-blende nanosystem, the contribution of acoustic phonons to the exciton-phonon interaction is smaller than that in the case of the wurtzite nanosystem. Calculations of the correlated exciton mass testify that the interaction of an exciton with acoustic phonons at all temperatures results in its increase by maximum 8% in the case of wurtzite nanosystems and by 5% in the case of zinc-blende nanosystems. We believe that the obtained theory and results of calculations will be useful both for a more complete and broader understanding of exciton-phonon interaction processes in nitride nanosystems as active elements of THz optoelectronic devices and for the further development of the theory of exciton-phonon interaction in geometric nanosystems of different symmetries.

DOI: [10.1103/PhysRevB.108.075403](https://doi.org/10.1103/PhysRevB.108.075403)**I. INTRODUCTION**

Electronic processes occurring in multilayer plane nitride nanostructures have direct practical applications in the operation of quantum cascade lasers (QCLs) and detectors (QCDs) [1–4]. The importance of the influence of phonons on these processes should be emphasized, that is, their impact on non-radiative transitions with energies being close to the energies of optical phonons to ensure the transport of a tunneled electron beam from one cascade of a nanodevice to another. For mono- or two-layer nanostructures and multilayer QCL and QCD cascades, created on the basis of arsenide or nitride semiconductor compounds, the spectra of optical phonons and their interaction with electrons have been investigated earlier [5–17]. For acoustic phonons, the problem of investigating their spectrum and interaction with electrons was considered

quite a long time ago [18–20] on the basis of finite difference method for single-well nanosystems and recently using a similar approach for multilayer nitride nanostructures [21]. In addition, the cases of such interaction both through the deformation and through the piezoelectric potential [19,20] were considered. As far as we know, the interaction of excitons with acoustic phonons in low-dimensional systems has not been studied thoroughly theoretically yet. This is due to a number of reasons, the main reason being the lack of an analytical theory of acoustic phonons in nitride nanosystems and an arbitrary number of semiconductor layers (this theory was proposed in Ref. [22]). As a result, the theoretical models applied mainly to the study of thermal conductivity of a nanostructure and the factors accompanying these phenomena, developed in Refs. [23–26], are based on the numerical solution of equations describing phonon modes. The second problem is the lack of a developed approach to the renormalization of the exciton spectrum. However, to single out a number of experimental papers where the exciton-phonon interaction in AlN/GaN nanostructures with different

^{*}boyko.i.v.theory@gmail.com; Ternopil Ivan Puluj National Technical University, Ternopil 46001, Ukraine.

geometrical symmetries was studied [27–31]. Moreover, attention should be paid to two theoretical papers [32,33], where the exciton-phonon interaction in anisotropic nonpolar 6H-SiC crystals was studied.

The direct focus on the investigation of acoustic phonons in the present paper is due to the reasons for the relevance of developing the theory of electron-phonon and exciton-phonon interaction, as well as the practical application of such a theory to real nanostructures, due to these main reasons. Plane resonant tunneling structures, which are precision elements of QCLs or QCDs, should provide coherent tunneling electron transport. Despite the fact that the operation of QCLs and QCDs is based only on electronic transitions, there are a number of papers [34–37] devoted to nanosystems in terms of their geometric and physical parameters, similar to the active elements of these nanodevices, but the subject of study in them are the exciton states. The present paper is motivated by the need to understand coherency in plane nanostructures' resonant tunneling transport, which required an understanding of exciton-phonon interactions. These interactions manifest themselves in a temperature shift and decay rate of the quantized levels. Among various electron-phonon and exciton-phonon scattering effects, we here focus on acoustic phonon interactions because the theory for it has been least developed in detail for nitrides and because they are the most relevant at low temperatures.

Thus, taking into account the current state of research, in our paper we propose an analytical theory of the exciton-phonon interaction in the case of acoustic phonons. The proposed paper is structured as follows: the theory of stationary states of electrons and holes, an exciton problem for nitride nanostructure, is considered in Sec. II. The theory of acoustic phonons and deformation and piezoelectric potentials created by them is presented in Sec. III A for zinc-blende nanosystems and in Sec. III B for wurtzite nanosystems, respectively. The theory of exciton-phonon interaction and renormalization of the exciton spectrum, based on the temperature Green's function method and the Dyson equation, is presented in Sec. IV. Analysis of the obtained theoretical results and calculations performed on the example of a nitride nanosystem is presented in Sec. V. Conclusions and most important results are presented in Sec. VI.

II. SPECTRUM AND WAVE FUNCTIONS OF AN ELECTRON AND A HOLE IN A MULTILAYER NANOSTRUCTURE

First, we will establish the electron and hole spectrum of the nanosystem under study. Its energy scheme, calculated for an electron and a hole, along with a coordinate system and notation for the boundaries between potential barriers and wells, is demonstrated in Fig. 1. The exciton Hamiltonian, in accordance with the notation in Fig. 1, is as shown:

$$H_{ex}(\rho, z_e, z_h) = E_g + \hat{H}_{(e)}(z_e) + \hat{H}_{(h)}(z_h) + \hat{H}_r(\rho, z_e, z_h) + V(|z_e - z_h|). \quad (1)$$

The Coulomb interaction between an electron and a hole in Eq. (1) is described by the constituent part of the Hamiltonian,

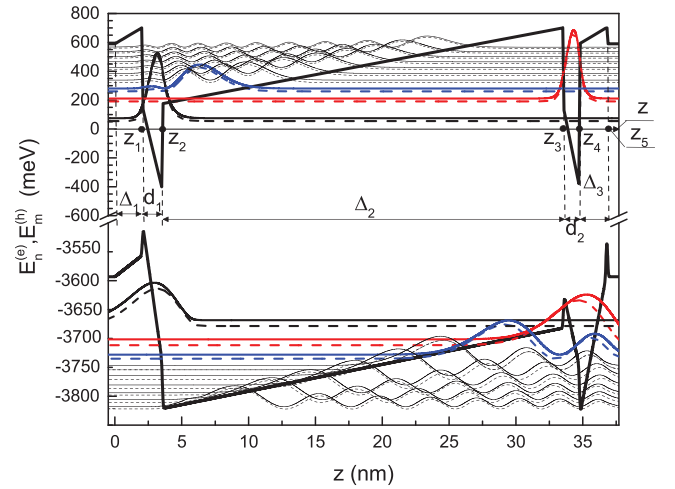


FIG. 1. The energy scheme of the nanosystem under study calculated for an electron and a hole, respectively, together with the squared moduli of their energy-level wave functions (solid lines correspond to wurtzite semiconductors, dashed lines correspond to zinc-blende semiconductors). The energy scale has a break in the range from -600 meV to -3500 meV. The values of the nanosystem layers from left to right in nanometers are as follows: **2.0/1.5/30.0/1.25/2.0** nm, where potential barriers are indicated in bold font.

which is defined as follows:

$$V(|z_e - z_h|) = -\frac{e^2}{4\pi\epsilon_0\epsilon^{(\alpha)}(z_\alpha)\sqrt{\rho^2 + (z_e - z_h)^2}}, \quad (2)$$

where ρ is the relative distance between an electron and a hole in a plane perpendicular to the Oz axis. To describe the relative motion of an electron and a hole, one should consider their motion in a coordinate system referred to their center of mass. Such motion is determined by the following component of the Hamiltonian:

$$\hat{H}_r(\rho, z_e, z_h) = -\frac{\hbar^2}{2\mu(z_e, z_h)}\left(\frac{\partial^2}{\partial\rho^2} + \frac{1}{\rho}\frac{\partial}{\partial\rho}\right), \quad (3)$$

where the reduced exciton mass is calculated as follows:

$$\mu(z_e, z_h) = \frac{m^{(e)}(z_e)m^{(h)}(z_h)}{m^{(e)}(z_e) + m^{(h)}(z_h)}. \quad (4)$$

The band gap as a function of temperature T is calculated from the Varshni formula,

$$E_g^{(*)}(T) = E_0^{(*)} - a^{(*)}T^2/(b^{(*)} + T), \quad (5)$$

$$E_0^{(*)} = E_g^{(*)}(T)|_{T=0}, \quad * = \{\text{AlN}, \text{GaN}\},$$

where $a^{(\alpha)}$, $b^{(\alpha)}$ are the Varshni parameters for AlN and GaN semiconductors. Since in the nanosystem under study, some of its layers are of a three-component semiconductor alloy, the band gap depending on the content x of the AlN semiconductor was calculated using the following condition:

$$E_g(x) = xE_g^{(\text{AlN})} + (1-x)E_g^{(\text{GaN})} + cx(1-x), \quad (6)$$

where c is a fitting parameter [38] which is different for wurtzite and zinc-blende layers. The energy scheme of the

nanosystem for the electron and hole without taking into account the influence of internal fields, i.e., strain-affected offsets for valance and conduction bands is calculated using Eqs. (5) and (6). This results are given in terms obtained by the ratio of the conduction band to the valence band offset:

$$U^{(e)}(z_e) = \begin{cases} 0, & \text{in GaN wells} \\ 0.765(E_g^{\text{AlGaIn}} - E_g^{\text{GaN}}), & \text{in AlGaIn,} \end{cases} \quad (7)$$

$$U^{(h)}(z_h) = \begin{cases} 0, & \text{in GaN wells} \\ 0.235(E_g^{\text{AlGaIn}} - E_g^{\text{GaN}}), & \text{in AlGaIn.} \end{cases}$$

Next, we will calculate the strength of the internal electric field that arises in the layers of the nanostructure due to the arising spontaneous and piezoelectric polarizations [39–42]. For this purpose, we will use the boundary conditions for the electric displacement field at the boundaries of the nanostructure ($\mathbf{D}_k = \mathbf{D}_{k+1}$, $\mathbf{D}_k = \varepsilon_k \mathbf{F}_k + \mathbf{P}_{\text{total}}^{(k)}$) and the condition imposed on the total potential drop on the entire nanosystem ($\sum_{k=1}^N F_k \Delta z^{(k)} = 0$) (see also Ref. [41]). This gives the following ratio:

$$F_p = \sum_{k=1; k \neq p}^N \frac{[P_{\text{total}}^{(k)} - P_{\text{total}}^{(p)}] \Delta z_{\alpha}^{(p)}}{\varepsilon_{(p)}^{(\alpha)} \varepsilon_{(k)}^{(\alpha)}} \bigg/ \sum_{k=1}^N \frac{\Delta z_{\alpha}^{(k)}}{\varepsilon_{(k)}^{(\alpha)}}, \quad (8)$$

where the indices p and k specify the labels of the nanosystem layers and, besides, p specifies the number of the layer in which the electric field is calculated, whereas summation takes place over the index k . The total polarization in Eq. (8) is $P_{\text{total}}^{(p)} = P_{\text{pz}}^{(p)} + P_{\text{sp}}^{(p)}$, $\Delta z_{\alpha}^{(p)} = z_{\alpha}^{(p-1)} - z_{\alpha}^{(p)}$ are the dimensions of the nanosystem layer in which the magnitude of the electric field strength is calculated, and the values $\varepsilon_{(p)}^{(\alpha)}$ specify the dielectric constant of this layer. In general, the permittivity of nanostructure, nanostructure density, electron and hole effective mass, and stiffness tensor can be presented as

follows:

$$A^{(\alpha)}(z_{\alpha}) = \sum_{p=0}^N A_p^{(\alpha)} [\theta(z_{\alpha} - z_{\alpha}^{(p)}) - \theta(z_{\alpha} - z_{\alpha}^{(p+1)})],$$

$$A^{(\alpha)} = [\varepsilon^{(\alpha)}(z_{\alpha}) m^{(\alpha)}(z_{\alpha}) C_{iklm}(z) \rho(z)]^T,$$

$$\alpha = \{e, h\}, \quad z_{\alpha}^{(N+1)} = +\infty, \quad (9)$$

where $\varepsilon_0^{(\alpha)}$, $\varepsilon_1^{(\alpha)}$ is the permittivity of AlN and AlGaIn semiconductors, respectively, $\theta(z)$ is the Heaviside unit function. Therefore, using the components $\hat{H}_{(e)}(z_e)$ and $\hat{H}_{(h)}(z_h)$ corresponding to the free electron and hole, taking into account Eqs. (7) and (8), we find separately the spectrum and wave functions of the free electron and hole. To do this, we find solutions to the stationary Schrödinger equation:

$$\left[-\frac{\hbar^2}{2} \frac{\partial}{\partial z_{\alpha}} \frac{1}{m^{(\alpha)}(z_{\alpha})} \frac{\partial}{\partial z_{\alpha}} + U^{(\alpha)}(z_{\alpha}) + U_E^{(\alpha)}(z_{\alpha}) \right] \Psi^{(\alpha)}(z_{\alpha}) = E^{(\alpha)} \Psi^{(\alpha)}(z_{\alpha}), \quad (10)$$

where

$$U_E^{(\alpha)}(z_{\alpha}) = \sum_{p=1}^N (-1)^{p-1} q^{(\alpha)} F_p \left(z_{\alpha} - \frac{F_{p-1} z_{\alpha}^{(p-1)}}{F_p} \right) \times [\theta(z_{\alpha} - z_{\alpha}^{(p-1)}) - \theta(z_{\alpha} - z_{\alpha}^{(p)})], \quad q^{(\alpha)} = \begin{cases} q^{(e)} = -e \\ q^{(h)} = e. \end{cases} \quad (11)$$

We calculate the wave functions of an electron and a hole in the model of a closed nanosystem. This directly means that the spectra of these quasiparticles are stationary. Thus, the obtained solutions of Eq. (10) are damped functions in the outer regions, relatively the nanosystem. Inside the nanosystem, taking into account that the potential $U_E^{(\alpha)}(z_{\alpha})$ Eq. (11) has a linear dependence on the coordinate z_{α} , we find that the solutions of the Schrödinger Eq. (10) in this case will be presented by linear combinations of the Airy functions $\text{Ai}(z_{\alpha})$ and $\text{Bi}(z_{\alpha})$ inside it [43]. Thus,

$$\Psi^{(\alpha)}(z_{\alpha}) = A_{(0)}^{\alpha} e^{\chi_{(0)}^{\alpha} z_{\alpha}} \theta(-z_{\alpha}) + B_{(N+1)}^{\alpha} e^{-\chi_{(N+1)}^{\alpha} z_{\alpha}} \theta(z_{\alpha} - z_{\alpha}^{(N+1)}) + \sum_{p=1}^N \{A_{(p)}^{\alpha} \text{Ai}[\zeta_{(p)}^{\alpha}(z_{\alpha})] + B_{(p)}^{\alpha} \text{Bi}[\zeta_{(p)}^{\alpha}(z_{\alpha})]\} [\theta(z_{\alpha} - z_{\alpha}^{(p-1)}) - \theta(z_{\alpha} - z_{\alpha}^{(p)})];$$

$$\zeta_{(p)}^{\alpha}(z_{\alpha}) = \sqrt[3]{\frac{2(-1)^{p-1} m_p^{(\alpha)} q^{(\alpha)} F_p}{\hbar^2} \left[\frac{U^{(\alpha)}(z_{\alpha}) - E}{q^{(\alpha)}} + (-1)^{p-1} (F_p z_{\alpha} - F_{p-1} z_{\alpha}^{(p-1)}) \right]};$$

$$\chi_{(0)}^{\alpha} = \chi_{(N+1)}^{\alpha} = \hbar^{-1} \sqrt{2m_0^{(\alpha)} (U^{(\alpha)}(z_{\alpha})|_{z_{\alpha} < 0, z_{\alpha} > z_{\alpha}^{(N+1)}} - E)}. \quad (12)$$

Next, we use the boundary conditions that describe the continuity of the wave function and flows of its probability density at all boundaries of the nanostructure,

$$\Psi_{(p)}^{\alpha}(E, z_{\alpha}^{(p)}) = \Psi_{(p+1)}^{\alpha}(E, z_{\alpha}^{(p)});$$

$$\frac{d\Psi_{(p)}^{\alpha}(E, z_{\alpha})}{m^{(\alpha)}(z_{\alpha}) dz_{\alpha}} \bigg|_{z=z_{\alpha}^{(p)}-0} = \frac{d\Psi_{(p+1)}^{\alpha}(E, z_{\alpha})}{m^{(\alpha)}(z_{\alpha}) dz_{\alpha}} \bigg|_{z=z_{\alpha}^{(p)}+0}, \quad (13)$$

then system Eq. (13) yields a dispersion equation, from which the discrete electron and hole spectra are determined (E_s^α , $s = (n, m)$, where the indices n and m are the numbers of the levels of the discrete spectrum of an electron and hole, respectively). Having applied boundary conditions Eq. (13), we will successively express the coefficients $A_{(0)}^\alpha$, $B_{(N+1)}^\alpha$, $A_{(p)}^\alpha$, $B_{(0)}^\alpha$ in solutions Eq. (12) in terms of one of them, which is chosen arbitrarily. This coefficient is obtained using the normalization condition

$$\int_{-\infty}^{+\infty} \Psi_s^{(\alpha)*}(E_s^\alpha, z_\alpha) \Psi_{s'}^{(\alpha)}(E_{s'}^\alpha, z_\alpha) dz_\alpha = \delta_{ss'}, \quad (14)$$

and thus the wave functions of a free electron and a hole are completely defined.

Therefore, to obtain the spectrum and wave functions of the exciton, one should find solutions to the stationary Schrödinger equation:

$$\hat{H}_{ex}(\rho, z_e, z_h) \Psi(\rho, z_e, z_h) = E_{ex} \Psi(\rho, z_e, z_h). \quad (15)$$

Equation (15) in the general case does not have an exact analytical solution, which is due to the complex form of the complete exciton Hamiltonian with a contribution describing the interaction of an electron and a hole. In this case, to perform the calculation of the exciton binding energy, we will provide the exciton wave function in the following way:

$$\Psi_{nm}(\rho, z_e, z_h) = \Psi_n^{(e)}(z_e) \Psi_m^{(h)}(z_h) \Phi(\rho), \quad (16)$$

where functions $\Phi(\rho)$ are selected as follows [44,45]:

$$\Phi(\rho) = \sqrt{\frac{2}{\pi}} \frac{e^{-\rho/\lambda}}{\lambda}, \quad (17)$$

where λ is a variation parameter. Now the exciton binding energy in the ground state will be determined from the minimization condition for the functional, relatively this parameter:

$$E_{nm}^{ex} = \min_{\lambda} \frac{\langle \Psi_{nm}(\rho, z_e, z_h) | \hat{H}_{ex}(\rho, z_e, z_h) | \Psi_{nm}(\rho, z_e, z_h) \rangle}{\langle \Psi_{nm}(\rho, z_e, z_h) | \Psi_{nm}(\rho, z_e, z_h) \rangle}. \quad (18)$$

Now using the exciton binding energy in the ground state obtained from Eq. (18), we calculate the exciton binding energy E_{nm}^b and the transition energy $E_{ph} = E_{nm}^{(e,h)}$ between an electron and a hole:

$$\begin{aligned} E_{nm}^b &= E_n^{(e)} + E_m^{(h)} - E_{nm}^{ex}; \\ E_{nm}^{(e,h)} &= E_n^{(e)} + E_m^{(h)} + E_g - E_{nm}^{ex}. \end{aligned} \quad (19)$$

Using the wave functions of an electron and a hole, we calculate the intensity of intersubband transitions:

$$I_{nm}^{(e-h)} = \left| \int_{-\infty}^{+\infty} \Psi_n^{(e)}(z) \Psi_m^{(h)}(z) dz \right|^2. \quad (20)$$

Let us now introduce for the exciton a quantized wave function as follows:

$$\hat{\Psi}(\rho, z_e, z_h) = \sum_{\mathbf{k}k_e, \mathbf{k}_h} \Psi_{\mathbf{k}k_e, \mathbf{k}_h}(\rho, z_e, z_h) \hat{a}_{\mathbf{k}k_e, \mathbf{k}_h}, \quad (21)$$

where

$$k_\alpha = \begin{cases} \chi_{(0)}^\alpha, & z_\alpha < 0, \quad z_\alpha > z_\alpha^{(N)} \\ \sqrt{2m_p^{(\alpha)}} [U^{(\alpha)}(z_\alpha^{(p)}) + U_E^{(\alpha)}(z_\alpha^{(p)})] / \hbar^2, & \\ 0 \leq z_\alpha \leq z_\alpha^{(N)}. & \end{cases} \quad (22)$$

Here $\hat{a}_{\mathbf{k}k_e, \mathbf{k}_h}$ is bosonic state annihilation operator with the commutation relation $[\hat{a}_{\mathbf{k}k_e, \mathbf{k}_h}, \hat{a}_{\mathbf{k}'k'_e, \mathbf{k}'_h}^\dagger] = \delta_{\mathbf{k}k_e, \mathbf{k}'_e} \delta_{\mathbf{k}_h, \mathbf{k}'_h} \delta_{\mathbf{k}, \mathbf{k}'}$; then the exciton Hamiltonian takes the canonical appearance,

$$\begin{aligned} \hat{H}_{ex} &= \int dz_e dz_h \hat{\Psi}^\dagger(\rho, z_e, z_h) H_{ex}(\rho, z_e, z_h) \hat{\Psi}(\rho, z_e, z_h) \\ &= \sum_{\mathbf{k}k_e, \mathbf{k}_h} \tilde{E}_{\mathbf{k}k_e, \mathbf{k}_h}(\mathbf{k}_e, \mathbf{k}_h) \hat{a}_{\mathbf{k}k_e, \mathbf{k}_h}^\dagger \hat{a}_{\mathbf{k}k_e, \mathbf{k}_h}, \end{aligned} \quad (23)$$

where $\tilde{E}_{\mathbf{k}k_e, \mathbf{k}_h}(\mathbf{k}_e, \mathbf{k}_h) = E_{\mathbf{k}k_e, \mathbf{k}_h}(\mathbf{k}_e, \mathbf{k}_h) + \hbar^2 k^2 / 2\mu(z_e, z_h)$ is the dispersion law for excitons in the state (k_e, k_h) , determined from the dispersion equation defined by conditions Eq. (10), where \mathbf{k} is the exciton quasimomentum, which acquires all values in the Brillouin zone.

III. SPECTRUM OF ACOUSTIC PHONONS OF A MULTILAYER NANOSTRUCTURE. DEFORMATION AND PIEZOELECTRIC POTENTIAL OF ACOUSTIC PHONONS IN THE CASE OF SEMICONDUCTORS OF WURTZITE AND ZINC-BLENDE CRYSTAL STRUCTURE

The piezoelectric effect due to the shear, as well as flexural and dilatational types of acoustic phonons, were studied in Refs. [46] and [19,47], respectively. However, this paper and relevant ones were devoted only to nitride nanosystems with a wurtzite-type crystal lattice, and such investigations were not carried out for the case of a zinc-blende-type crystal lattice. Therefore, we will focus only on the main points of calculating the components of acoustic phonons for different types of crystal lattices and the deformation and piezoelectric potentials created by them.

Let us use the equation of motion for an elastic semiconductor continuum, which is presented as follows:

$$\begin{aligned} \rho(z) \frac{\partial^2 u_i(\mathbf{r}, t)}{\partial t^2} &= \frac{\partial \sigma_{ik}(\mathbf{r}, t)}{\partial x_k}; \quad \mathbf{r} = \mathbf{r}_{||} + \mathbf{e}_z z, \quad i, \\ k &= (1; 2; 3), \end{aligned} \quad (24)$$

where the stress tensor is $\sigma_{ik}(r) = C_{iklm}(z) [\partial u_i(\mathbf{r}) / \partial x_k + \partial u_k(\mathbf{r}) / \partial x_i] / 2$. It provides the equation

$$\rho(z) \frac{\partial^2 u_i(\mathbf{r}, t)}{\partial t^2} - \frac{\partial}{\partial x_k} \left\{ \frac{C_{iklm}(z)}{2} \left[\frac{\partial u_i(\mathbf{r})}{\partial x_k} + \frac{\partial u_k(\mathbf{r})}{\partial x_i} \right] \right\} = 0. \quad (25)$$

A. Theory of the acoustic phonons modes and the piezoelectric potential created by them in the case of the zinc-blende crystal lattice type

As far as we know, for nitride nanostructures with a zinc blende crystal lattice, the theory of both acoustic phonons and the piezoelectric potential is not available. Since the stiffness

tensor and the piezoelectric tensor are

$$C_{ij}^{ZB(p)} = \begin{pmatrix} C_{11}^{(p)} & C_{12}^{(p)} & C_{12}^{(p)} & 0 & 0 & 0 \\ C_{12}^{(p)} & C_{11}^{(p)} & C_{12}^{(p)} & 0 & 0 & 0 \\ C_{12}^{(p)} & C_{12}^{(p)} & C_{11}^{(p)} & 0 & 0 & 0 \\ 0 & 0 & 0 & C_{44}^{(p)} & 0 & 0 \\ 0 & 0 & 0 & 0 & C_{44}^{(p)} & 0 \\ 0 & 0 & 0 & 0 & 0 & C_{44}^{(p)} \end{pmatrix};$$

$$e_{ij}^{ZB(p)} = \begin{pmatrix} 0 & 0 & 0 & e_{14}^{(p)} & 0 & 0 \\ 0 & 0 & 0 & 0 & e_{14}^{(p)} & 0 \\ 0 & 0 & 0 & 0 & 0 & e_{14}^{(p)} \end{pmatrix}, \quad (26)$$

which is fundamentally different from similar tensors for a wurtzite-type crystal lattice, one should expect differences in

$$D(q, z) = \begin{bmatrix} -C_{44}^{(p)} \frac{d^2}{dz^2} + q^2 C_{11}^{(p)} & 0 & iq(C_{12}^{(p)} + C_{44}^{(p)}) \frac{d}{dz} \\ 0 & -C_{44}^{(p)} \frac{d^2}{dz^2} + q^2 C_{44}^{(p)} & 0 \\ iq(C_{12}^{(p)} + C_{44}^{(p)}) \frac{d}{dz} & 0 & -C_{11}^{(p)} \frac{d^2}{dz^2} + q^2 C_{44}^{(p)} \end{bmatrix}. \quad (29)$$

Now, from Eq. (28), taking into account Eq. (29), we obtain equations describing the flexural and dilatational phonon modes:

$$-\frac{d^2 u_{1(3)}^{(p)}(z)}{dz^2} + iq c_{1(3)}^{(p)} \frac{du_{3(1)}^{(p)}(z)}{dz} + (\chi_{1(3)}^{(p)})^2 u_{1(3)}^{(p)}(z) = 0;$$

$$c_{1(3)}^{(p)} = (C_{12}^{(p)} + C_{44}^{(p)}) C_{44(11)}^{(p)};$$

$$\chi_{1(3)}^{(p)} = \sqrt{(q^2 C_{11}^{(p)} - \rho^{(p)} \omega^2) C_{44(11)}^{(p)}}, \quad (30)$$

$$u_1^{(p)}(z) = -iq c_1^{(p)} \sum_{s=1}^2 \left(A_{2s-1}^{(p)} e^{\lambda_s^{(p)} z} - A_{2s}^{(p)} e^{-\lambda_s^{(p)} z} \right) / \|u_s^{(p)}(q)\|;$$

$$u_3^{(p)}(z) = - \sum_{s=1}^2 \left\{ (\lambda_s^{(p)})^2 + (\chi_1^{(p)})^2 \right\} \left(A_{2s-1}^{(p)} e^{\lambda_s^{(p)} z} + A_{2s}^{(p)} e^{-\lambda_s^{(p)} z} \right) / \|u_s^{(p)}(q)\|, \quad (32)$$

$$\|u_s^{(p)}(q)\| = \sqrt{|q c_1^{(p)} \lambda_s^{(p)}|^2 + |(\lambda_s^{(p)})^2 + (\chi_1^{(p)})^2|^2}, \quad u_2^{(p)}(z) = A_2^{(p)} e^{-\chi z} + B_2^{(p)} e^{\chi z}, \quad \chi = \sqrt{q^2 - \frac{\rho^{(p)} \omega^2}{C_{44}^{(p)}}},$$

where $\lambda_s^{(p)}$ are the roots of the biquadratic equation $\lambda^4 + [(\chi_1^{(p)})^2 + (\chi_3^{(p)})^2 + q^2 c_1^{(p)} c_3^{(p)}] \lambda^2 + (\chi_1^{(p)} \chi_3^{(p)})^2 = 0$; moreover, here $\lambda_1^{(p)} = -\lambda_3^{(p)}$; $\lambda_2^{(p)} = -\lambda_4^{(p)}$.

The coefficients in the first two solutions Eq. (32) are found from the boundary conditions,

$$u_{1(3)}^{(p)}(q, z)|_{z=z_p-0} = u_{1(3)}^{(p+1)}(q, z)|_{z=z_p+0};$$

$$\sigma_{13(33)}^{(p)}(q, z)|_{z=z_p-0} = \sigma_{13(33)}^{(p+1)}(q, z)|_{z=z_p+0}, \quad (33)$$

where the Cauchy stress tensor components are as follows:

$$\sigma_{13}^{(p)}(q, z) = \frac{1}{2} C_{44}^{(p)} \left(-iqu_3^{(p)}(z) + \frac{du_1^{(p)}(z)}{dz} \right) e^{i(\mathbf{q}\mathbf{r}_{\parallel} - \omega t)},$$

the formation of deformation and piezoelectric potentials and their effect on the exciton spectrum.

The solutions of Eq. (25), taking into account Eq. (26), will be presented as follows:

$$u_\ell(\mathbf{r}, t) = u_\ell(q, z) e^{i(\mathbf{q}\mathbf{r}_{\parallel} - \omega t)}, \quad \ell = 1, 2, 3, \quad q = \sqrt{q_x^2 + q_y^2}, \quad (27)$$

which after simple transformations results in the following matrix equation:

$$\rho^{(p)} \omega^2 u_\ell^{(p)}(q, z) - D^{(p)}(q, z) u_\ell^{(p)}(q, z) = 0, \quad (28)$$

with a differential operator of the following appearance:

as well as the shear phonon modes:

$$\frac{d^2 u_2^{(p)}(z)}{dz^2} - \left(q^2 - \frac{\rho^{(p)} \omega^2}{C_{44}^{(p)}} \right) u_2^{(p)}(z) = 0. \quad (31)$$

System Eq. (30) is structurally similar to the system that arises in the theory of acoustic phonons in nitride nanosystems with a wurtzite-type lattice [18,19,21,22]. Using the method developed by us in Ref. [22] (based on application Cayley–Hamilton theorem), we obtain the final analytical solution:

$$\sigma_{33}^{(p)}(q, z) = \left(-iq C_{12}^{(p)} u_1^{(p)}(z) + C_{11}^{(p)} \frac{du_3^{(p)}(z)}{dz} \right) e^{i(\mathbf{q}\mathbf{r}_{\parallel} - \omega t)}, \quad (34)$$

combined with the normalization condition:

$$\frac{2S_{\perp} \omega}{\hbar} \int_{-\infty}^{+\infty} \rho(z) [u_1(q, \omega_q, z) u_1^*(q', \omega_q', z) + u_3(q, \omega_q, z) u_3^*(q', \omega_q', z)] = \delta_{qq'}; \quad S_{\perp} = \Delta l_x \Delta l_y. \quad (35)$$

In addition, conditions Eq. (33) give a dispersion equation that determines the phonon spectrum $\Omega_{n_1}^{ac} = \hbar \omega_{n_1}$. Similarly, using the boundary conditions for the components $u_2(q, z)$; $\sigma_{23}(q, z)$, we find the spectrum of shear phonons.

Now our goal is to get an equation for determining the piezoelectric potential. To do this, we use the fact that the displacement vector is defined as

$$\mathbf{D}(\mathbf{r}, t) = -\varepsilon_0 \varepsilon(z) \nabla \phi_{\text{pz}}^{\text{ZB}}(\mathbf{r}, t) + \mathbf{P}_{\text{pz}}^{\text{ZB}}(\mathbf{r}, t) + \mathbf{P}_{\text{sp}}. \quad (36)$$

It should be taken into account that the spontaneous polarization is directed along the z axis ($\mathbf{P}_{\text{sp}} = P_{\text{sp}} \mathbf{k}$), and the piezoelectric polarization is defined as follows [we immediately pass to the Voigt notation, since Eq. (26)]:

$$\begin{aligned} \mathbf{P}_{\text{pz}}^{\text{ZB}} &= e_{klm} \varepsilon_{lm} = e_{ij}^{\text{ZB}}(z) (\varepsilon_{11} \varepsilon_{22} \varepsilon_{33} \ 2\varepsilon_{23} \ 2\varepsilon_{13} \ 2\varepsilon_{12})^T \\ &= 2e_{14}(z) (\varepsilon_{23} \ \varepsilon_{13} \ \varepsilon_{12})^T, \ \varepsilon_{ij} = \varepsilon_{ij}(\mathbf{r}, t). \end{aligned} \quad (37)$$

We now use the explicit form for phonon modes Eq. (32) to calculate the magnitudes of the strain tensor components ε_{ij} . Moreover, we will take into account the fact that the nanosystem is not affected by from external distributed charges, which according to the Maxwell's equation gives

$$\rho_{\text{ext}} = (\nabla \cdot \mathbf{D}) = 0. \quad (38)$$

Having substituted expressions Eqs. (37) and (38) into Eq. (36), we obtain the equation which describes piezoelectric

potential:

$$-\varepsilon_0 \nabla [\varepsilon(z) \nabla \phi_{\text{pz}}^{\text{ZB}}(\mathbf{r}, t)] + \nabla [2e_{14}(z) (\varepsilon_{23} \ \varepsilon_{13} \ \varepsilon_{12})^T] = 0. \quad (39)$$

It should be noted that in Eq. (39) there is no contribution from spontaneous polarization. Next we write this equation for a single layer of the nanosystem, and perform the Fourier transform for the components of phonon modes, as well as for the generated deformation and piezoelectric potentials according to the relations

$$\begin{aligned} u_\ell(q, \omega_{n_1 q}, \mathbf{r}, t) &= \sum_{n_1 q} u_\ell(q, \omega_{n_1 q}, z) e^{i(\mathbf{q}\mathbf{r} - \omega_{n_1 q} t)}; \\ \phi_{\text{pz}}^{\text{ZB}}(q, \omega_q, \mathbf{r}, t) &= \sum_{n_1 q} \phi_{\text{pz}}^{\text{ZB}}(q, \omega_{n_1 q}, z) e^{i(\mathbf{q}\mathbf{r} - \omega_{n_1 q} t)}, \end{aligned} \quad (40)$$

then we will obtain

$$\begin{aligned} -\varepsilon_0 \varepsilon^{(p)} \nabla^2 \phi_{\text{pz}}^{\text{ZB}}(\mathbf{r}, t) \\ + 4e_{14}^{(p)} \left(\frac{\partial^2 u_1(\mathbf{r}, t)}{\partial y \partial z} + \frac{\partial^2 u_2(\mathbf{r}, t)}{\partial x \partial z} + \frac{\partial^2 u_3(\mathbf{r}, t)}{\partial x \partial y} \right) = 0. \end{aligned} \quad (41)$$

Next, it is convenient to pass from the obtained Fourier components to generalized coordinates and momenta, and then to the occupation number operators, since, for the example in Ref. [44,47], we obtain the operator for phonon modes in the representation of occupation numbers:

$$\begin{aligned} \hat{u}_\ell(q, \omega_{n_1 q}, r) &= \sum_{p=0}^N \sum_{n_1 q} \sqrt{\frac{\hbar}{2S_\perp \rho^{(p)} \omega_{n_1 q}}} [\hat{b}_{n_1}^+(-\mathbf{q}) + \hat{b}_{n_1}(\mathbf{q})] \hat{w}_\ell^{(p)}(q, \omega_{n_1 q}, z) e^{i\mathbf{q}\mathbf{r}} [\theta(z - z_p) - \theta(z - z_{p+1})], \\ \hat{w}_\ell^{(p)}(q, \omega_{n_1 q}, z) &= \sqrt{\rho^{(p)}} \hat{u}_\ell^{(p)}(q, \omega_{n_1 q}, z), \ z_0 = 0; \ z_{N+1} = +\infty. \end{aligned} \quad (42)$$

Then, using Eqs. (32), (42) and separating the equation for the component $\varphi_{\text{pz}}^{\text{ZB}}(z) = \varphi_{\text{pz}}^{\text{ZB}}(q, \omega_q, z)$ in Eq. (41), we find [see also Eq. (A1)]

$$\begin{aligned} \frac{d^2 \varphi_{\text{pz}}^{\text{ZB}}(z)}{dz^2} - q^2 \varphi_{\text{pz}}^{\text{ZB}}(z) - \frac{e_{14}^{(p)}}{\varepsilon_0 \varepsilon^{(p)}} \sqrt{\frac{8\hbar}{S_\perp \rho^{(p)} \omega_{n_1 q}}} \\ \times \left[q_x q_y w_3^{(p)}(z) - i \left(q_y \frac{dw_1^{(p)}(z)}{dz} + q_x \frac{dw_2^{(p)}(z)}{dz} \right) \right] = 0. \end{aligned} \quad (43)$$

To determine the coefficients $A^{(p)}$, $B^{(p)}$, the boundary conditions for the potential $\varphi_{\text{pz}}^{\text{ZB}}(z)$ and electric displacement $D_{\text{pz}}^{\text{ZB}}(z) = \varepsilon_0 \varepsilon(z) d\varphi_{\text{pz}}^{\text{ZB}}(z)/dz$ are used:

$$\begin{aligned} \phi_{\text{pz}}^{\text{ZB}(p)}(z) \Big|_{z \rightarrow z_p - 0} &= \phi_{\text{pz}}^{\text{ZB}(p+1)}(z) \Big|_{z \rightarrow z_p + 0}, \\ \varepsilon(z) d\phi_{\text{pz}}^{\text{ZB}(p)}(z) / dz \Big|_{z \rightarrow z_p + 0} &= \varepsilon(z) d\phi_{\text{pz}}^{\text{ZB}(p+1)}(z) / dz \Big|_{z \rightarrow z_p + 0}. \end{aligned} \quad (44)$$

By calculating the deformation potential for the entire valence band, we obtain

$$\begin{aligned} \phi_{\text{def}}^{\text{ZB}}(q, \omega_q, \mathbf{r}, t) &= \Delta E_C^{\text{ZB}}(\mathbf{r}, t) = a_C^{\text{ZB}} [\varepsilon_{11}(\mathbf{r}, t) + \varepsilon_{22}(\mathbf{r}, t) + \varepsilon_{33}(\mathbf{r}, t)] \\ &= \left\{ \frac{a_C^{\text{ZB}}}{\|u_s^{(p)}(q)\|} \sqrt{\frac{\hbar}{2S_\perp \omega_{n_1 q}}} \sum_{s=1}^2 [qq_x c_1^{(p)} + \lambda_s^{(p)} \{(\lambda_s^{(p)})^2 + (\chi_1^{(p)})^2\}] (A_{2s-1}^{(p)} e^{\lambda_s^{(p)} z} + A_{2s}^{(p)} e^{-\lambda_s^{(p)} z}) \right. \\ &\quad \left. + a_C^{\text{ZB}} q_y (A_2^{(p)} e^{-\chi z} + B_2^{(p)} e^{\chi z}) \right\} e^{i(\mathbf{q}\mathbf{r} - \omega t)} = \sum_{n_1 q} \phi_{\text{pz}}^{\text{ZB}}(q, \omega_{n_1 q}, z) e^{i(\mathbf{q}\mathbf{r} - \omega t)}, \end{aligned} \quad (45)$$

where $a_C^{\text{ZB}} = a_C$ is the deformation potential constant for the valence band.

Consequently, the Hamiltonians describing the interaction with phonons in terms of the piezoelectric and deformation potentials in the case of a zinc-blende-type lattice are as follows:

$$\begin{aligned}\hat{H}_{\text{pz}} &= \sum_{q n_1} \sum_{p=1}^2 \sum_{s=1}^2 \left[A^{(p)} e^{qz} + B^{(p)} e^{-qz} - \frac{e^{(p)}}{\varepsilon_0 \varepsilon^{(p)} q} \sqrt{\frac{2\hbar}{S_{\perp} \rho^{(p)} \omega_{n_1 q}}} \left\{ e^{qz} \int_0^z e^{-q\xi} \Phi_s^{(p)}(q, \xi) d\xi \right. \right. \\ &\quad \left. \left. - e^{-qz} \int_0^z e^{q\xi} \Phi_s^{(p)}(q, \xi) d\xi \right\} \right] [\hat{b}_{n_1}^+(-\mathbf{q}) + \hat{b}_{n_1}(\mathbf{q})] e^{i\mathbf{q}\mathbf{r}} [\theta(z - z_p) - \theta(z - z_{p+1})]; \\ \hat{H}_{\text{def}} &= a_C^{\text{ZB}} \sum_{q n_1} \sum_{p=1}^2 \sum_{s=1}^2 \sqrt{\frac{\hbar}{2 \|u_s^{(p)}(q)\|^2 S_{\perp} \omega_{n_1 q}}} [qq_x c_1^{(p)} + \lambda_s^{(p)} \{(\lambda_s^{(p)})^2 + (\chi_1^{(p)})^2\}] (A_{2s-1}^{(p)} e^{\lambda_s^{(p)} z} + A_{2s}^{(p)} e^{-\lambda_s^{(p)} z}) \\ &\quad + q_y (A_2^{(p)} e^{-\lambda z} + B_2^{(p)} e^{\lambda z}) [\hat{b}_{n_1}^+(-\mathbf{q}) + \hat{b}_{n_1}(\mathbf{q})] e^{i\mathbf{q}\mathbf{r}} [\theta(z - z_p) - \theta(z - z_{p+1})].\end{aligned}\quad (46)$$

B. Theory of modes of acoustic phonons and the piezoelectric potential created by them in the case of the wurtzite-type crystal lattice

For nanosystems with a wurtzite crystal lattice, we developed a theory of acoustic phonons [22]. But taking into account the form of the elastic constant tensor, the equations for phonon modes can be easily obtained without using the results of Ref. [22] from Eq. (30) by replacing: $C_{12}^{(p)} \rightarrow C_{13}^{(p)}$; $C_{44}^{(p)} \rightarrow C_{66}^{(p)}$; $C_{11}^{(p)} \rightarrow C_{33}^{(p)}$. In addition, in the last equation of Eq. (30) there must be $(q^2 - \rho^{(p)} \omega^2 / C_{44}^{(p)}) \rightarrow (q^2 C_{66}^{(p)} / C_{44}^{(p)} - \rho^{(p)} \omega^2 / C_{44}^{(p)})$. Then, for the nanosystem under study, solutions of Eq. (30) $\tilde{u}_1^{(p)}$, $\tilde{u}_2^{(p)}$, $\tilde{u}_3^{(p)}$ can be represented similar to (32) [see Eq. (A2)].

Now the piezoelectric polarization, taking into account the Voigt notation, will be defined as follows:

$$\begin{aligned}P_{\text{pz}}^{\text{WZ}} &= e_{klm} \varepsilon_{lm} = e_{ij}^{\text{WZ}}(z) (\varepsilon_{11} \varepsilon_{22} \varepsilon_{33} 2\varepsilon_{23} 2\varepsilon_{13} 2\varepsilon_{12})^T \\ &= \begin{bmatrix} 2e_{15}(z) \varepsilon_{13} \\ 2e_{15}(z) \varepsilon_{23} \\ e_{31}(z) (\varepsilon_{11} + \varepsilon_{22}) + e_{33}(z) \varepsilon_{33} \end{bmatrix}, \varepsilon_{ij} = \varepsilon_{ij}(\mathbf{r}, t).\end{aligned}\quad (47)$$

Now using equation this solutions Eq. (A2) in relation $\mathbf{D}(\mathbf{r}, t) = -\varepsilon_0 \varepsilon(z) \nabla \phi_{\text{pz}}^{\text{WZ}}(\mathbf{r}, t) + \mathbf{P}_{\text{pz}}^{\text{WZ}}(\mathbf{r}, t) + \mathbf{P}_{\text{sp}}$, taking into account expressions Eq. (47), we obtain

$$\begin{aligned}-\varepsilon_0 \nabla [\varepsilon(z) \nabla \phi_{\text{pz}}^{\text{WZ}}(r, t)] + \nabla [2e_{15}(z) \varepsilon_{13} 2e_{15}(z) \varepsilon_{23} e_{31}(z) \\ \times (\varepsilon_{11} + \varepsilon_{22}) + e_{33}(z) \varepsilon_{33}]^T = 0,\end{aligned}\quad (48)$$

taking into account the fact that $\phi_{\text{pz}}^{\text{WZ}}(r, t) = \phi_{\text{pz}}^{\text{WZ}}(z) e^{i(qr - \omega t)}$ giving the following equation for a separate layer of the nanosystem:

$$\begin{aligned}-\varepsilon_0 \varepsilon^{(p)} \nabla^2 \phi_{\text{pz}}^{\text{WZ}}(\mathbf{r}, t) + (e_{15}^{(p)} + e_{31}^{(p)}) \left(\frac{\partial^2 u_1}{\partial x \partial z} + \frac{\partial^2 u_2}{\partial y \partial z} \right) \\ + e_{15}^{(p)} \left(\frac{\partial^2 u_3}{\partial x^2} + \frac{\partial^2 u_3}{\partial y^2} \right) + e_{31}^{(p)} \frac{\partial^2 u_3}{\partial z^2} = 0.\end{aligned}\quad (49)$$

Having substituted Eqs. (42) and (A2), we obtain an equation for the component $\phi_{\text{pz}}^{\text{WZ}}(z) = \phi_{\text{pz}}^{\text{WZ}}(q, \omega_q, z)$ [see also Eq. (A3)]:

$$\begin{aligned}\frac{d^2 \phi_{\text{pz}}^{\text{WZ}}(z)}{dz^2} - q^2 \phi_{\text{pz}}^{\text{WZ}}(z) \\ = \frac{1}{\varepsilon_0 \varepsilon^{(p)}} \sqrt{\frac{\hbar}{2 S_{\perp} \rho^{(p)} \omega_{n_1 q}}} \left[i(e_{15}^{(p)} + e_{31}^{(p)}) \left(q_x \frac{dw_1^{(p)}(z)}{dz} + q_y \frac{dw_2^{(p)}(z)}{dz} \right) + e_{15}^{(p)} q^2 w_3^{(p)}(z) - e_{31}^{(p)} \frac{d^2 w_3^{(p)}(z)}{dz^2} \right] = 0.\end{aligned}\quad (50)$$

For the deformation potential, we obtain in our case the following expression:

$$\begin{aligned}\phi_{\text{def}}^{\text{WZ}}(q, \omega_q, \mathbf{r}, t) = \Delta E_C^{\text{WZ}}(\mathbf{r}, t) = (a_{1C} - D_1) \varepsilon_{33}(\mathbf{r}, t) + (a_{2C} - D_2) (\varepsilon_{11}(\mathbf{r}, t) + \varepsilon_{22}(\mathbf{r}, t)) \\ = \sqrt{\frac{\hbar}{2 S_{\perp} \omega_{n_1 q}}} \left\{ \sum_{s=1}^2 [(a_{2C} - D_2) q q_x c_1^{(p)} - (a_{1C} - D_1) \lambda_s^{(p)} \{(\lambda_s^{(p)})^2 + (\chi_1^{(p)})^2\}] \right. \\ \times (\tilde{A}_{2s-1}^{(p)} e^{\lambda_s^{(p)} z} - \tilde{A}_{2s}^{(p)} e^{-\lambda_s^{(p)} z}) / \|u_s^{(p)}(q)\| \\ \left. + q_y (\tilde{A}_2^{(p)} e^{-\lambda z} + \tilde{B}_2^{(p)} e^{\lambda z}) \right\} e^{i(\mathbf{q}\mathbf{r} - \omega t)} = \sum_{n_1 q} \phi_{\text{def}}^{\text{WZ}}(q, \omega_{n_1 q}, z) e^{i(\mathbf{q}\mathbf{r} - \omega t)},\end{aligned}\quad (51)$$

where a_{1C} , a_{2C} , D_1 , D_2 - are the deformation potential constants for the valence band.

Thus, the Hamiltonians describing the interaction with phonons in terms of the deformation and piezoelectric potentials in the case of a wurtzite-type lattice are as follows:

$$\begin{aligned}\hat{H}_{\text{pz}}^{\text{WZ}} &= \sum_{q n_1} \sum_{p=1}^N \sum_{s=1}^2 \left(\tilde{A}^{(p)} e^{qz} + \tilde{B}^{(p)} e^{-qz} - \frac{1}{\varepsilon_0 \varepsilon^{(p)}} \sqrt{\frac{\hbar}{2S_{\perp} \rho^{(p)} \omega_{n_1 q}}} \left\{ e^{qz} \int_0^z e^{-q\xi} \tilde{\Phi}_s^{(p)}(q, \xi) d\xi \right. \right. \\ &\quad \left. \left. - e^{-qz} \int_0^z e^{q\xi} \tilde{\Phi}_s^{(p)}(q, \xi) d\xi \right\} [\hat{b}_{n_1}^+(-\mathbf{q}) + \hat{b}_{n_1}(\mathbf{q})] e^{i\mathbf{q}\mathbf{r}} [\theta(z - z_p) - \theta(z - z_{p+1})]; \\ \hat{H}_{\text{def}}^{\text{WZ}} &= \sum_{q n_1} \sum_{p=1}^N \sum_{s=1}^2 \sqrt{\frac{\hbar}{2 \|u_s^{(p)}(q)\|^2 S_{\perp} \omega_{n_1 q}}} \{ [(a_{2C} - D_2) q q_x c_1^{(p)} - (a_{1C} - D_1) \lambda_s^{(p)} \{ (\lambda_s^{(p)})^2 + (\chi_1^{(p)})^2 \}] \\ &\quad \times (\tilde{A}_{2s-1}^{(p)} e^{\lambda_s^{(p)} z} - \tilde{A}_{2s}^{(p)} e^{-\lambda_s^{(p)} z}) + q_y (\tilde{A}_2^{(p)} e^{-\tilde{\lambda} z} + \tilde{B}_2^{(p)} e^{\tilde{\lambda} z}) \} [\hat{b}_{n_1}^+(-\mathbf{q}) + \hat{b}_{n_1}(\mathbf{q})] e^{i\mathbf{q}\mathbf{r}} [\theta(z - z_p) - \theta(z - z_{p+1})],\end{aligned}\quad (52)$$

where the coefficients $\tilde{A}^{(p)}$, $\tilde{B}^{(p)}$ are found from the conditions similar to the conditions Eq. (44).

IV. HAMILTONIAN OF THE EXCITON-PHONON SYSTEM. RENORMALIZATION OF THE EXCITON SPECTRUM BY INTERACTION WITH ACOUSTIC PHONONS. CORRELATED EFFECTIVE MASS OF THE EXCITON TAKING INTO ACCOUNT THE EXCITON-PHONON INTERACTION

We start using bosonic operators $\hat{b}_{n_1}^+$ and \hat{b}_{n_1} representing the phonon Hamiltonian as follows:

$$\hat{H}_{\text{ph}}^{\text{ac}} = \sum_{n_1 \mathbf{q}} \hbar \omega_{n_1 \mathbf{q}} \left(\hat{b}_{n_1 \mathbf{q}}^+ \hat{b}_{n_1 \mathbf{q}} + \frac{1}{2} \right), \quad [\hat{b}_{n_1 \mathbf{q}}^+, \hat{b}_{n_1' \mathbf{q}'}] = \delta_{n_1 n'} \delta_{\mathbf{q} \mathbf{q}'} \quad (53)$$

Next, the renormalized positions of the ground and excited electronic states, the exciton lifetimes in these states, and the effect of phonons on the effective exciton mass are studied. It is assumed that the system has a weak exciton-phonon coupling. It should be mentioned that the exciton band is separated from other bands in such a way that their influence is that which can be neglected.

To obtain the Hamiltonian describing the interaction of excitons with acoustic phonons, in this case it will be assumed that an electron and a hole interact independently with acoustic phonons through the mechanisms of both deformation and piezoelectric potentials established above. It results in the following Hamiltonians describing this interaction:

$$\begin{aligned}\hat{H}_{\text{ex-ph}}^{\text{def(pz)}} &= \int dr_e dr_h \hat{\Psi}^+(\rho, r_e, r_h) (\hat{H}_{e-\text{ph}}^{\text{def(pz)}} + \hat{H}_{h-\text{ph}}^{\text{def(pz)}}) \hat{\Psi}(\rho, r_e, r_h) \\ &= \sum_{\mathbf{k} \mathbf{k}_e \mathbf{k}_h q n_1} F_{\mathbf{k} \mathbf{k}_e \mathbf{k}_h q n_1}^{\text{def(pz)}} \hat{a}_{\mathbf{k} + \mathbf{q} \mathbf{k}_e \mathbf{k}_h}^+ \hat{a}_{\mathbf{k} \mathbf{k}_e \mathbf{k}_h} [\hat{b}_{n_1}^+(-\mathbf{q}) + \hat{b}_{n_1}(\mathbf{q})],\end{aligned}\quad (54)$$

where the corresponding binding functions are calculated using expressions Eqs. (45), (46), (51), and (52) due to the relations

$$\begin{aligned}F_{\mathbf{k} \mathbf{k}_e \mathbf{k}_h q n_1}^{\text{def(pz)}} &= \sum_{p=1}^N \left[\iint |\Phi^{(p)}(\rho)|^2 d\rho^2 \int_{z_{p-1}}^{z_p} \Psi_{(p)}^{(e)}(E_{\mathbf{k} \mathbf{k}_e}, z_e) (\Psi_{(p)}^{(e)}(E_{\mathbf{k} \mathbf{k}_e}, z_e))^* dz_e \right. \\ &\quad \left. \times \int_{z_{p-1}}^{z_p} \Psi_{(p)}^{(h)}(E_{\mathbf{k} \mathbf{k}_h}, z_h) \phi_{\text{def(pz)}}^{\text{ZB(WZ)}}(q, \omega_{n_1 q}, z_h) e^{i\mathbf{q}\mathbf{r}_h} (\Psi_{(p)}^{(h)}(E_{\mathbf{k} \mathbf{k}_h}, z_h))^* dz_h \right] [\theta(z - z_p) - \theta(z - z_{p+1})], \quad z_{N+1} = +\infty.\end{aligned}\quad (55)$$

So, the complete Hamiltonian of the Wannier-Mott exciton system with acoustic phonons is as follows:

$$\begin{aligned}\hat{H} &= \hat{H}_{\text{ex}} + \hat{H}_{\text{ph}}^{\text{ac}} + \hat{H}_{\text{ex-ph}}^{\text{def}} + \hat{H}_{\text{ex-ph}}^{\text{pz}} = \sum_{\mathbf{k} \mathbf{k}_e \mathbf{k}_h} E_{\mathbf{k} \mathbf{k}_e \mathbf{k}_h}(\mathbf{k}_e, \mathbf{k}_h) \hat{a}_{\mathbf{k} \mathbf{k}_e \mathbf{k}_h}^+ \hat{a}_{\mathbf{k} \mathbf{k}_e \mathbf{k}_h} + \sum_{n_1 \mathbf{q}} \hbar \omega_{n_1 \mathbf{q}} \left(\hat{b}_{n_1 \mathbf{q}}^+(-\mathbf{q}) \hat{b}_{n_1 \mathbf{q}}(\mathbf{q}) + \frac{1}{2} \right) \\ &\quad + \sum_{\mathbf{k} \mathbf{k}_e \mathbf{k}_h q n_1} [F_{\mathbf{k} \mathbf{k}_e \mathbf{k}_h q n_1}^{\text{def}} + F_{\mathbf{k} \mathbf{k}_e \mathbf{k}_h q n_1}^{\text{pz}}] \hat{a}_{\mathbf{k} + \mathbf{q} \mathbf{k}_e \mathbf{k}_h}^+ \hat{a}_{\mathbf{k} \mathbf{k}_e \mathbf{k}_h} [\hat{b}_{n_1}^+(-\mathbf{q}) + \hat{b}_{n_1}(\mathbf{q})].\end{aligned}\quad (56)$$

Let us now introduce the retarded temperature Green's function of the exciton state, built on the stationary states of the electron $|n\rangle$ and hole $|m\rangle$, respectively, and n and m are the numbers of the levels of the spectrum of these quasiparticles. It is defined as

follows:

$$G_{nm}(\mathbf{k}, \omega') = \{\hbar\omega' - \tilde{E}_{\mathbf{k}\mathbf{k}_e\mathbf{k}_h}(\mathbf{k}_e, \mathbf{k}_h) - M(\mathbf{k}, \omega')\}^{-1}, \omega' = \omega + i\eta, \eta \rightarrow 0. \quad (57)$$

The mass operator in Eq. (57), which takes into account the contribution from the one-phonon process is obtained as follows:

$$M(\mathbf{k}, \omega') = \sum_{q n_1} F_{\mathbf{k}_e\mathbf{k}_h q n_1}^{\text{def(pz)}}(q) [F_{n_1 \mathbf{q} \mathbf{k}_h \mathbf{k}_e}^{\text{def(pz)}}(q)]^* \left\{ \frac{1 + v_{n_1}(q)}{\hbar\omega' - E_{\mathbf{k}\mathbf{k}_e\mathbf{k}_h}(\mathbf{k}_e, \mathbf{k}_h) - \hbar^2(\mathbf{k} - \mathbf{q})^2 / 2\mu(z_e, z_h) - \Omega_{n_1}(q)} + \frac{v_{n_1}(q)}{\hbar\omega' - E_{\mathbf{k}\mathbf{k}_e\mathbf{k}_h}(\mathbf{k}_e, \mathbf{k}_h) - \hbar^2(\mathbf{k} + \mathbf{q})^2 / 2\mu(z_e, z_h) + \Omega_{n_1}(q)} \right\}. \quad (58)$$

The value $v_{n_1}(q) = \{\exp(\Omega_{n_1}(q)/k_B T) - 1\}^{-1}$ is the average value of the occupation numbers of the acoustic phonons in the state with number n_1 .

Using the mass operator Eq. (58), the temperature dependence of the exciton states is calculated, which is determined by the basic shape function for the light absorption band, following the general theory of excitons [48], which is determined as follows:

$$I(\mathbf{k}, \xi, T) = \frac{\rho(\mathbf{k}, \xi, T)}{2} = - \frac{\text{Im}M(\mathbf{k}, \xi)}{[\xi - \tilde{E}_{\mathbf{k}\mathbf{k}_e\mathbf{k}_h}(\mathbf{k}_e, \mathbf{k}_h) - \text{Re}(\mathbf{k}, \xi)]^2 + [\text{Im}M(\mathbf{k}, \xi)]^2}, \xi = \hbar\omega. \quad (59)$$

Let us take into account the fact that the discrete part of the spectrum is renormalized in the case of weak exciton-phonon interaction. To specify the influence of this factor, we perform the Fourier transform of the Green's function Eq. (57), passing from summation over the wave vector q to integration by the rule $\sum_{\mathbf{q}} \Rightarrow S_{\perp} / (2\pi)^2 \iint d^2\mathbf{q}$ and using the Dirac relation:

$$\iint \frac{d^2\mathbf{q}}{F(q) + i\eta} = \mathcal{P} \iint \frac{d^2\mathbf{q}}{F(q)} - i\pi \iint \delta[F(q)] d^2\mathbf{q}, \quad (60)$$

where \mathcal{P} is a symbol for an integral calculated in the sense of Cauchy principal value. The shifts Δ_{nm} and decay rates γ_{nm} obtained from the dispersion equation $\hbar\omega' - \tilde{E}_{nm} - M(\mathbf{k}, \omega') = 0$ are as follows:

$$\begin{aligned} \Delta_{nm} &= \text{Re}M(\mathbf{k}, \omega')|_{\mathbf{k}=0} = \frac{S_{\perp}}{(2\pi)^2} \sum_{\tilde{n}\tilde{m}} \sum_{n_1} \mathcal{P} \iint \left[v_{n_1}(q) + \frac{1}{2} \pm \frac{1}{2} \right] \frac{F_{\mathbf{k}_e\mathbf{k}_h q n_1}^{\text{def(pz)}}(q) [F_{n_1 \mathbf{q} \mathbf{k}_h \mathbf{k}_e}^{\text{def(pz)}}(q)]^*}{E_{nm} - E_{\tilde{n}\tilde{m}q} + \Omega_{n_1}(q)} d^2\mathbf{q}; \\ \gamma_{nm} &= -2\text{Im}M(\mathbf{k}, \omega')|_{\mathbf{k}=0} \\ &= \frac{S_{\perp}}{2\pi} \sum_{\tilde{n}\tilde{m}} \sum_{n_1} \mathcal{P} \iint \left[v_{n_1}(q) + \frac{1}{2} \pm \frac{1}{2} \right] F_{\mathbf{k}_e\mathbf{k}_h q n_1}^{\text{def(pz)}}(q) [F_{n_1 \mathbf{q} \mathbf{k}_h \mathbf{k}_e}^{\text{def(pz)}}(q)]^* \delta[E_{nm} - E_{\tilde{n}\tilde{m}q} + \Omega_{n_1}(q)] d^2\mathbf{q}. \end{aligned} \quad (61)$$

In addition, our goal is to study the effect of temperature on the effective exciton mass in the nanostructure under study. As it is known from experimental and partially theoretical papers [27–29] that the presence of temperature does not result in a strong extinction of the exciton band; then, in this case, the description of the exciton as a quasiparticle remains valid, moreover, we can neglect the imaginary part of the mass operator Eq. (58). Let us now expand the equation obtained from the pole of the Green's function for the exciton Eq. (57) into a series in terms of the quasi-momentum \mathbf{k} , while retaining only the quadratic term:

$$\begin{aligned} \hbar\omega' - \tilde{E}_{nm} - \frac{\hbar^2 \mathbf{k}^2}{2\mu} - \text{Re}M(\mathbf{k}, \omega')|_{\mathbf{k}=0} \\ - \frac{\partial^2 M(\mathbf{k}, \omega')}{\partial \mathbf{k}^2} \Big|_{\mathbf{k}=0} \mathbf{k}^2 = 0; \mu = \mu(z_e, z_h). \end{aligned} \quad (62)$$

Therefore, the renormalized value of the effective exciton mass is as follows:

$$\tilde{\mu} = \frac{\mu}{1 + \partial^2 M(\mathbf{k}, \omega') / \partial \mathbf{k}^2 \Big|_{\mathbf{k}=0}} \quad (63)$$

and the renormalized exciton dispersion law looks like

$$\tilde{E}_{nm} = E_{nm} + \text{Re}M(\mathbf{k}, \omega')|_{\mathbf{k}=0} + \frac{\hbar^2 \mathbf{k}^2}{2\tilde{\mu}}. \quad (64)$$

V. RESULTS AND DISCUSSION

The calculations were performed using the geometric parameters of a nitride nanosystem with geometric parameters typical for recently created quantum cascade detectors [4]. In accordance with the notation of the coordinate system presented in Fig. 1, the nanosystem consists of three $\text{Al}_{0.4}\text{Ga}_{0.6}\text{N}$ potential barriers of $\Delta_1 = 2.0$ nm, $\Delta_2 = 30.0$ nm, $\Delta_3 = 2.0$ nm thickness and two GaN potential wells of $d_1 = 1.5$ nm and $d_2 = 1.25$ nm width, respectively. The physical parameters (which are taken from Refs. [34,38,49,50]) used in the calculations are similar to those presented in Tables I and II (the effective masses of an electron m_e^* and a hole m_h^* are given in units of the mass of a free electron m_e). The choice of just these geometric parameters of the studied nanostructure and the approach to performing calculations described below is due to the fact that considerable attention is paid to short-period quantum cascade detectors, the cascades of

TABLE I. Physical parameters of the GaN and $\text{Al}_{0.4}\text{Ga}_{0.6}\text{N}$ wurzite semiconductors.

Material	m_e^*	m_h^*	$\rho(\text{kg/m}^3)$	$C_{11}(\text{GPa})$	$C_{12}(\text{GPa})$	$C_{13}(\text{GPa})$	$C_{33}(\text{GPa})$	$C_{44}(\text{GPa})$	$C_{66}(\text{GPa})$
GaN	0.186	0.270	6150	390	145	106	398	105	122.5
$\text{Al}_{0.4}\text{Ga}_{0.6}\text{N}$	0.266	0.342	4992	392.4	141.8	106.8	388	109.4	129.5
Material	$e_{33}(\text{C/m}^2)$	$e_{31}(\text{C/m}^2)$	$e_{15}(\text{C/m}^2)$	$a_{1c}(\text{eV})$	$a_{2c}(\text{eV})$	$D_1(\text{eV})$	$D_2(\text{eV})$		
GaN	0.73	-0.49	-0.40	-4.9	-11.3	-3.7	8.2		
$\text{Al}_{0.4}\text{Ga}_{0.6}\text{N}$	1.06	-0.53	-0.43	-4.3	-11.5	-9.1	8.4		

which are usually nanostructures with two or three potential wells [4,51,52]. It makes it possible to study sequentially a number of typical nanostructure configurations, the often considered cases of nanosystems with a single potential well, in particular.

The energy scheme of the nanosystem calculated for an electron and a hole, together with all the discrete spectra (E_n , E_m) of these quasiparticles formed by size quantization are presented in Fig. 1. Here we present the results of calculations for semiconductors with both a wurzite-type lattice (solid lines) and a zinc-blende-type lattice (dashed lines). For clarity of the presented results, the energy scale is detailed and has a break from -600 meV to -3500 meV. As can be seen from Fig. 1 in the nanosystem under study in both cases, there are ten electronic and nine hole discrete stationary levels available. In this case, the energies of electrons and holes for semiconductors of the two types considered are close, but in the case of a wurzite-type lattice, they are somewhat higher than in the case of a zinc-blende type. The localization of these electron and hole states is shown by the squared moduli of the wave functions given for each of the states. It should be noted that the oscillating part of the electron wave functions is located above the potential line, while in the case of holes it is located below the potential line. As can be seen from Fig. 1, the oscillating parts of the electronic functions end at the point corresponding to the intersection with the potential line, while for holes this point actually corresponds to their beginning.

We will carry out subsequent calculations of the studied physical quantities as follows. We fix the value of the thickness of potential barriers and perform calculations in such a way that the value of the left potential well changes from 0 to $d_1 + d_2$, and the value of the right well changes from $d_1 + d_2$ to 0. Then, in fact, the value of $0 \leq d \leq d_1 + d_2$ will specify the position of the internal potential barrier regarding external ones. It should also be noted that the trivial case of a nanosystem with one quantum well can also be obtained in our calculations, moreover, this case is always presented on the calculated dependencies at $d \rightarrow 0$ and $d \rightarrow d_1 + d_2$. In addition, we will further assume that the value $d^{(\text{exp})}$ indicated on the dependencies given in the paper corresponds to the above parameters of the nanosystem geometric configuration.

This principle of calculation clearly demonstrates the spectrum of electron and hole states of the nanosystem under study, calculated as a function of the value of d , which is presented in Fig. 2. The scale break in this figure is in the range -100 meV to -3600 meV. As can be seen from Fig. 2 in this approach, one can clearly observe the formation of the bottleneck effect in the calculated dependencies for stationary electronic states, and this effect is the most evident for the lower levels of the spectrum. Thus, considering how the hole states of the nanostructure are localized (in fact, in the area of the internal potential barrier), it is obvious that the hole energy levels do not actually depend on the value of d , which is confirmed by the calculated dependencies in Fig. 2, which are almost straight lines. It should also be noted that for wurzite and zinc-blende type semiconductors, the dependencies of both quasiparticles on d are similar.

Before proceeding to the study of the acoustic phonons' influence on exciton states of the nanosystem, let us find out the etymology of the formation for the values of the deformation

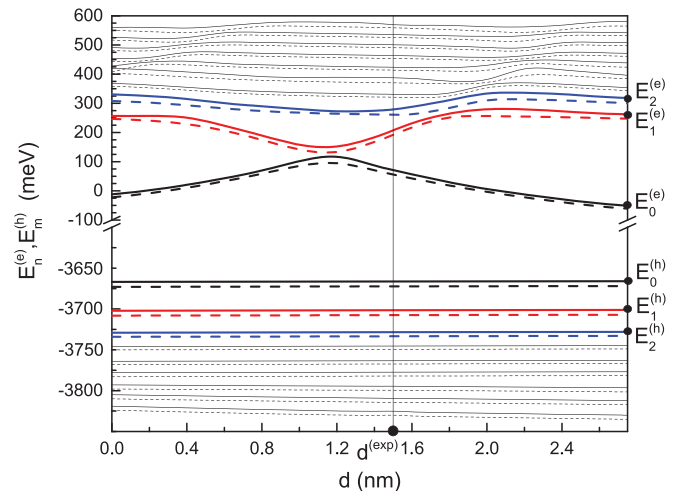


FIG. 2. The electron $E_n^{(e)}$ and hole $E_m^{(h)}$ spectra calculated as functions of the internal barrier position ($0 \leq d \leq d_1 + d_2$) in the total potential well (solid lines correspond to wurzite semiconductors, dashed lines correspond to zinc blende semiconductors). The energy scale has a break in the range from -100 meV to -3600 meV.

TABLE II. Physical parameters of the GaN and $\text{Al}_{0.4}\text{Ga}_{0.6}\text{N}$ zinc-blende semiconductors.

Material	m_e^*	m_h^*	$\rho(\text{kg/m}^3)$	$C_{11}(\text{GPa})$	$C_{12}(\text{GPa})$	$C_{44}(\text{GPa})$	$e_{14}(\text{C/m}^2)$	$a_c(\text{eV})$
GaN	0.190	0.290	6150	293	159	159	0.50	-6.71
$\text{Al}_{0.4}\text{Ga}_{0.6}\text{N}$	0.246	0.362	4992	297.4	159.4	172.6	0.54	-5.8

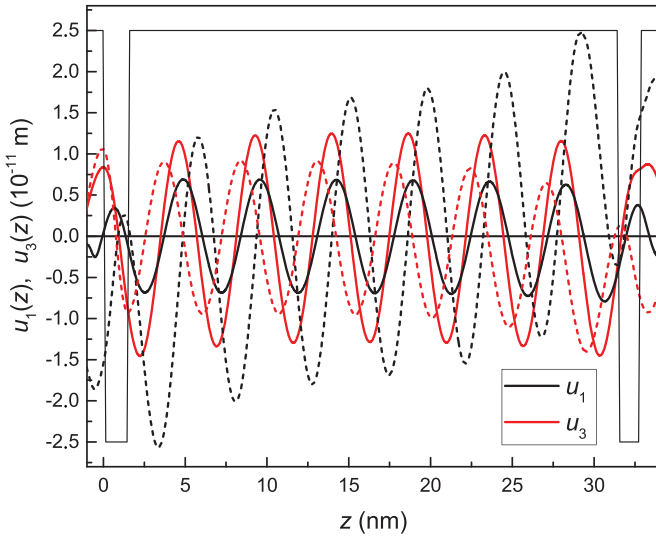


FIG. 3. Displacements $u_1(z)$ (black lines) and $u_3(z)$ (red lines) localized in the nanosystem at $q_x = q_y = q = 10 \text{ nm}^{-1}$ (solid lines correspond to wurtzite semiconductors, dashed lines correspond to zinc-blende semiconductors).

and piezoelectric potentials in the studied nanosystem. For this purpose, we calculated the values of the displacements u_1 and u_3 included in the mentioned potentials according to expressions Eqs. (44), (45), (51), and (52). An example of the result of such calculations for u_1 and u_3 , when they are localized within the entire area of the nanosystem, is presented in Fig. 3, respectively, for wurtzite semiconductors (solid lines) and zinc-blende semiconductors (dashed lines). The energies' acoustic phonon spectrum obtained from the dispersion equation determined by the boundary conditions Eq. (33) must satisfy the limits of application of the elastic continuum model, which imposes a condition on their value: $\Omega_{n_1}^{ac} \leq 35 \text{ meV}$ [18–20,22]. Taking this fact into account and without loss of generality, to establish differences between the dependencies obtained for different types of crystal structure, the value of the wave number were taken fixed: $q_x = q_y = q = 10 \text{ nm}^{-1}$. In this case, the calculated acoustic phonon energies belong to the interval from 10 meV to 29 meV. As can be seen from Fig. 3, the dependencies u_1 and u_3 testify a similar behavior, forming the same number of nodes in the nanostructure region, but they differ in amplitude and phase both among themselves and in both cases of the crystal structure of semiconductors.

Further, the results presented in Fig. 4 demonstrate the behavior of the deformation and piezoelectric potentials in the area of the nanosystem. These quantities were calculated for the same value of the wave number $q_x = q_y = q$. As can be seen from Fig. 4, all potential values acquire only negative values inside the nanosystem, having a clear tendency to decrease from left to right in the scale of z values. In this case, the largest modulo value of the studied potentials is formed in the region of the right quantum well at the boundary with the initial potential barrier. As can be seen from Fig. 4, in the case when the nanosystem is formed by wurtzite-type semiconductors, the absolute values of the deformation potential dominate the absolute values of the piezoelectric potential by 2–5 times.

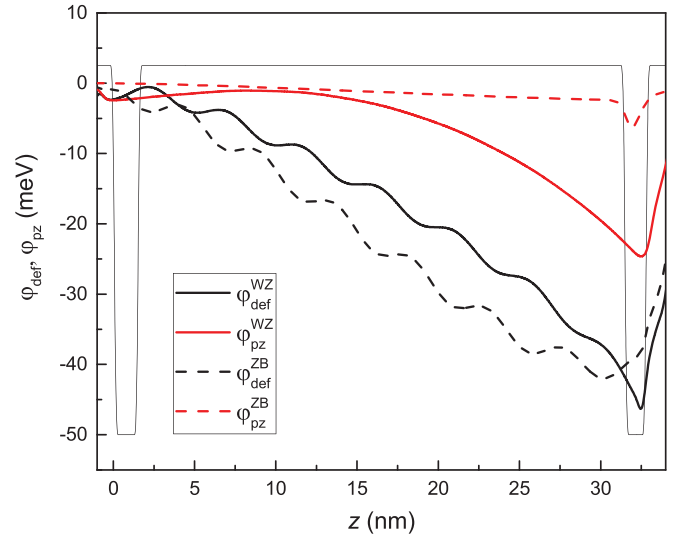


FIG. 4. Deformation potential (black lines) and piezoelectric potential (red lines) calculated at $q_x = q_y = q = 10 \text{ nm}^{-1}$ (solid lines correspond to wurtzite semiconductors, dashed lines correspond to zinc blende semiconductors).

However, in the case of a zinc-blende nanosystem, this fact is not satisfied: the value of the deformation potential is the dominant value, exceeding the equal absolute value of the piezoelectric potential by 18–20 times. We obtain that the established fact remains valid for all nanosystem configurations determined in our calculations by the value $0 \leq d \leq d_1 + d_2$ introduced above. Thus, we can conclude that in the case of a wurtzite nanosystem, the effect of acoustic phonons on exciton states is due to both deformation and piezoelectric potentials, while in the case of a zinc-blende nanosystem, the exciton–phonon interaction is determined mainly by the deformation potential.

Taking into account the localization of electron and hole states in the nanosystem, in further calculations we calculate the displacements Δ_{nm} and decay rates γ_{nm} for the first three exciton states ($n = m = 0..2$). At the same time, the temperature range from 50 K to 300 K will be relevant for us, which will make it possible to cover a variety of temperature conditions for existing semiconductor devices. To compare, we will first consider the dependencies for displacements $\Delta_{nm} = \Delta_{nm}(d)$ for different types of crystal lattices, and then, in the same vein, we will analyze the dependencies for $\gamma_{nm} = \gamma_{nm}(d)$.

Figures 5(a)–5(f) present the results of calculating the shifts of the exciton spectrum, which were performed for four temperature values: 50 K, 100 K, 200 K, 300 K. Figures 5(a)–5(c) correspond to the case of wurtzite semiconductors (WZ), and Figs. 5(d)–5(f) correspond to zinc-blende semiconductors (ZB), respectively. As can be seen from the given dependencies $\Delta_{nm} = \Delta_{nm}(d)$ in the low-temperature regime (50 K), all shifts have a negative sign, i.e., the interaction with acoustic phonons results in a shift of exciton energy levels to lower energies range. At the same time, we do not set ourselves the task of considering the simplest case when $T = 0 \text{ K}$; moreover, this case cannot be obtained by passing to the limit $T \rightarrow 0 \text{ K}$ within the proposed theory. It should be noted that increasing

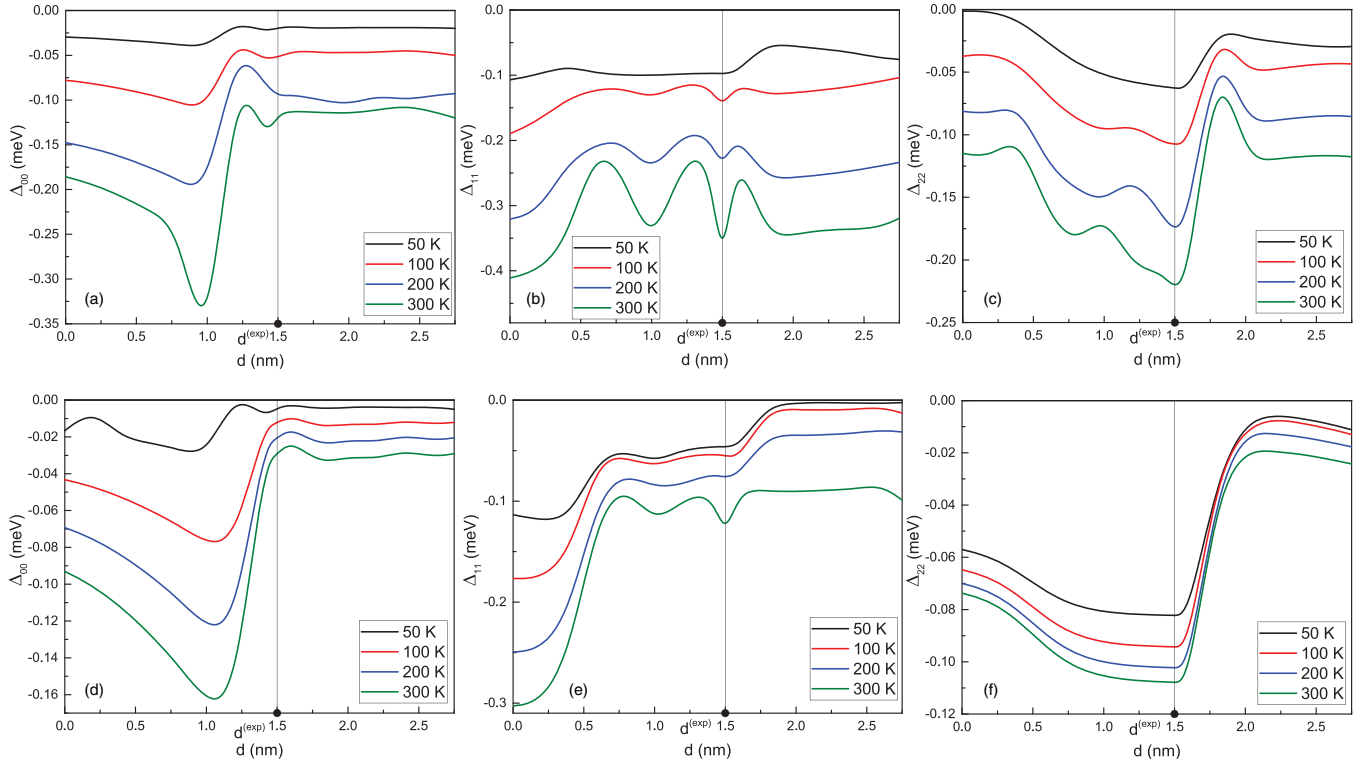


FIG. 5. Shifts of the exciton spectrum calculated as functions of d for various temperatures. (a)–(c) correspond to a wurtzite semiconductors and (d)–(f) correspond to a zinc-blende semiconductors.

temperature does not result in an increase in the absolute values of the shifts and the formation in the dependencies' $\Delta_{nm}(d)$ intervals of d values, in which the values of the shifts depend on d sufficiently and such intervals, where such dependence is not great. For example, for $\Delta_{00}^{\text{WZ}}(d)$ and $\Delta_{00}^{\text{ZB}}(d)$, this interval of strong dependence on d is actually the same: $0 \text{ nm} \leq d \leq 1.3 \text{ nm}$, however, in the case of $\Delta_{00}^{\text{WZ}}(d)$ the maximum absolute value of the shift at $T = 300 \text{ K}$ is two times greater than in the case of $\Delta_{00}^{\text{ZB}}(d)$. In the interval $1.5 \text{ nm} \leq d \leq 2.75 \text{ nm}$, both values of shifts depend on d insufficiently. It can be seen from Figs. 5(b) and 5(e) that the dependencies of the shifts $\Delta_{11}^{\text{WZ}}(d)$ and $\Delta_{11}^{\text{ZB}}(d)$ are quite similar to each other in the interval $0 \text{ nm} \leq d \leq 0.35 \text{ nm}$. For the remaining values of d , it is clear that $\Delta_{11}^{\text{WZ}}(d) > \Delta_{11}^{\text{ZB}}(d)$. Taking into account now the dependencies in Figs. 5(c) and 5(f), it is established that the shifts $\Delta_{22}^{\text{WZ}}(d)$ and $\Delta_{22}^{\text{ZB}}(d)$ in a narrow interval $1.45 \text{ nm} \leq d \leq 1.55 \text{ nm}$ form its maximum absolute values. In addition, despite the formal similarity of the dependencies, Δ_{22}^{WZ} are clearly different from each other: $\Delta_{11}^{\text{ZB}}|_{T=300 \text{ K}} > \Delta_{11}^{\text{ZB}}|_{T=200 \text{ K}} > \Delta_{11}^{\text{ZB}}|_{T=100 \text{ K}} > \Delta_{11}^{\text{ZB}}|_{T=50 \text{ K}}$, and in the case of Δ_{22}^{ZB} the values are quite close to each other for all temperature values.

Further in Figs. 6(a)–6(f), the results of calculations and the decay rates for exciton states are presented, the shift of which was calculated above. The temperature values at which the calculations were performed are the same as in the case of the dependencies presented in Fig. 5. As can be seen from the comparisons of Fig. 6(a)–6(c) and Figs. 6(d)–6(f), they are quite similar to the case of both types of crystal lattice, but a number of differences should be noted. The maximum

values of decay rates are somewhat higher for the case of wurtzite semiconductors; moreover, the temperature increase does not affect the dependencies for zinc-blende semiconductors to a less extent, which at all temperatures will remain symmetrical relative to the value $d = (d_1 + d_2)/2$. Special attention is paid to providing the condition: $\gamma_{nm}^{\text{WZ(ZB)}}|_{T=50 \text{ K}} < \gamma_{nm}^{\text{WZ(ZB)}}|_{T=100 \text{ K}} < \gamma_{nm}^{\text{WZ(ZB)}}|_{T=200 \text{ K}} < \gamma_{nm}^{\text{WZ(ZB)}}|_{T=300 \text{ K}}$ for all possible nanosystem configurations d . Having summarized the dependency analysis in Figs. 5 and 6, it should be concluded that the lower absolute values of shifts and decay rates in the case of zinc-blende semiconductors are due to the dominance of only the mechanism of interaction with acoustic phonons through the deformation potential, while in the case of wurtzite semiconductors, both mechanisms of such interaction are beneficial, which, in fact was predicted by analyzing the dependencies in Fig. 4.

Further, the dependencies presented in Fig. 7 result in calculations for the energies of electron-hole transitions and exciton basic band-shape function, which were calculated for the above temperatures in the vicinity of these energy values. As can be seen from Fig. 7(a), the energies of electron-hole transitions in the case of zinc-blende-type semiconductors somewhat predominate on results obtained in the case of wurtzite-type semiconductors, and the dependencies on d themselves are quite similar. The values of these energies, obtained at $d = d^{\text{exp}}$, to be clear, correspond to the values of the maxima of the exciton basic band-shape function L_{11} , L_{22} , L_{33} . It can be seen from Figs. 7(b) and 7(c) that the dependencies L_{11} , L_{22} , L_{33} on energy ξ are of quasi-Lorentz curves. With the temperature increase, the effect of the widths increase for the obtained curves and a decrease of their

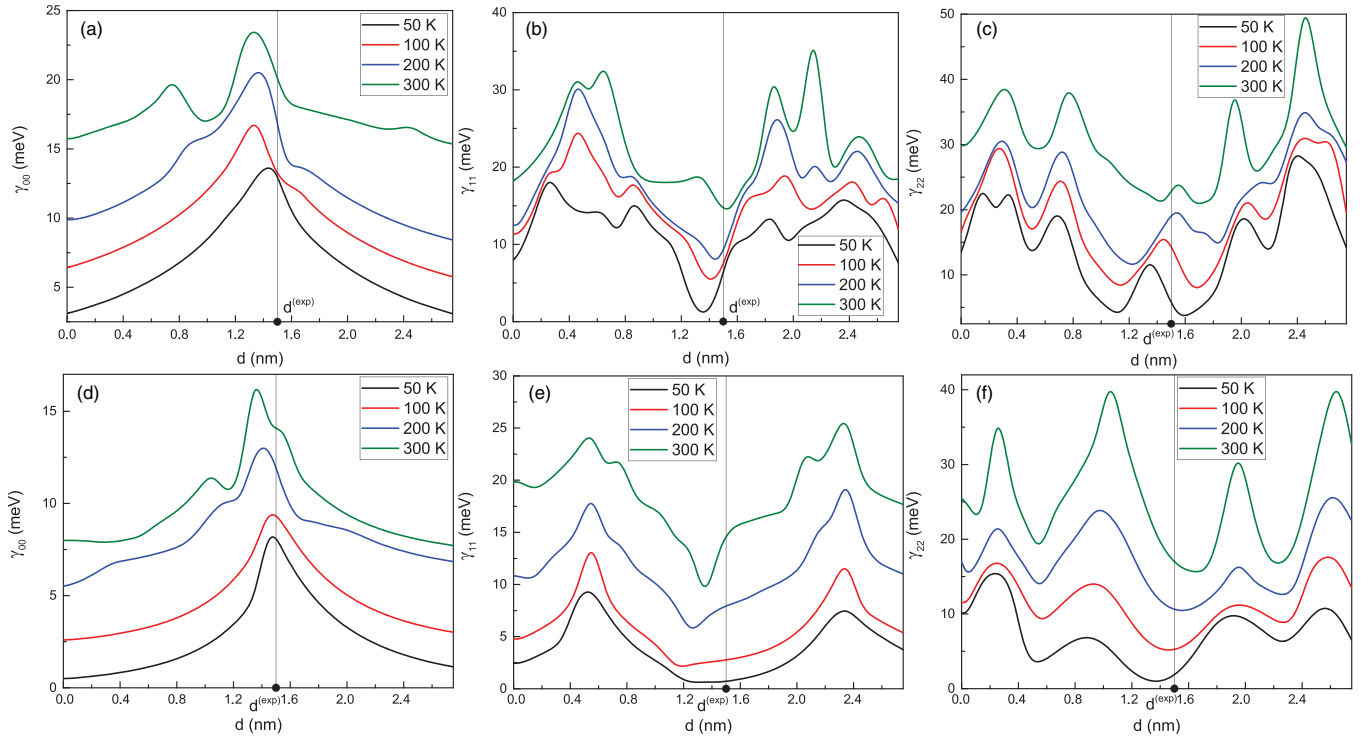


FIG. 6. Decay rates of the exciton states calculated as functions of d for various temperatures. (a)–(c) correspond to a wurtzite semiconductors and (e)–(f) correspond to a zinc-blende semiconductors.

maxima values is observed, which is additionally explained by the dependencies shown in Fig. 6. It should be noted that for all calculated temperature values, the maximum value of the function $L_{nm}(\xi)$ is always observed in the case of a nanostructure based on zinc-blende semiconductors. This is explained by the effect established above, when for zinc-blende-type semiconductors, the contribution of acoustic phonons to the exciton-phonon interaction is mainly due to the deformation potential and is smaller than in the case of wurtzite semiconductors. In addition, as seen from Figs. 6(c) and 6(d), at $T = 50$ K the following condition is satisfied: $L_{nm}(\xi)|_{T=50\text{ K}} \gg L_{nm}(\xi)|_{T=100\text{ K}}, L_{nm}(\xi)|_{T=200\text{ K}}, L_{nm}(\xi)|_{T=300\text{ K}}$. Thus, we can say that there is an approximation to the theory at $T = 0$ K

when $\gamma_{nm} = 0$, according to the general theory of excitons [45], however, it is clear that we do not mean the direct convergence of these results and the theory at $T = 0$ K should be considered separately.

At the final stage, we will study the effect of acoustic phonons on the renormalization of the exciton effective mass in the nanosystem under study. Since the effective mass of an exciton is different in different semiconductor layers, then in relation Eq. (65) we will consider the value of the reduced mass of the exciton μ the value of its mass averaged over the contribution of the layers of the nanosystem (this approach was used in Ref. [53] for the electronic problem). In our case, the expression for the average exciton mass is as follows:

$$\langle \mu \rangle = \langle \mu_{nm} \rangle = \left[\int_{-\infty}^{+\infty} \frac{\{m^{(e)}(z_e) + m^{(h)}(z_h)\} |\Psi_n^{(e)}(z_e)|^2 dz_e \int_{-\infty}^{+\infty} \frac{|\Psi_m^{(e)}(z_h)|^2 dz_h}{m^{(h)}(z_h)} \right]^{-1}. \quad (65)$$

In addition, expression Eq. (64) clearly shows that the average exciton mass depends on the numbers n and m of the corresponding bound electron and hole states.

In Fig. 8, the temperature dependencies of the average effective exciton masses are presented, demonstrating their renormalization due to the influence of acoustic phonons for a nanosystem with wurtzite and zinc-blende semiconductor layers, respectively. As can be seen from Fig. 8, the exciton effective masses $\langle \mu_{11} \rangle$, $\langle \mu_{22} \rangle$, $\langle \mu_{33} \rangle$ are close to each other at $T = 50$ K. In this case, for all temperature values, the following condition is satisfied: $\langle \mu_{11} \rangle > \langle \mu_{22} \rangle > \langle \mu_{33} \rangle$ and always $\langle \mu_{nm}^{\text{WZ}} \rangle > \langle \mu_{nm}^{\text{ZB}} \rangle$, and the observed effect is an increase

of the exciton effective mass due to the exciton-phonon interaction. It should be noted that at temperatures $T < 200$ K the dependencies of $\langle \mu_{11} \rangle$ on T are of a quadratic type, which is weakly expressed for $\langle \mu_{22} \rangle$ and even weaker for $\langle \mu_{33} \rangle$. At temperatures $T > 200$ K, a quasilinear dependence of the renormalized effective exciton masses on temperature is already observed, which is a consequence of the actual implementation of the approximation: $v_{n_1}(q) \approx k_B T / \Omega_{n_1}(q)$. In general, it should be noted that in the case of wurtzite semiconductors, the renormalized effective mass of an exciton increases more than in the case of semiconductors of the zinc-blende type [54] and amounts to the maximum possible

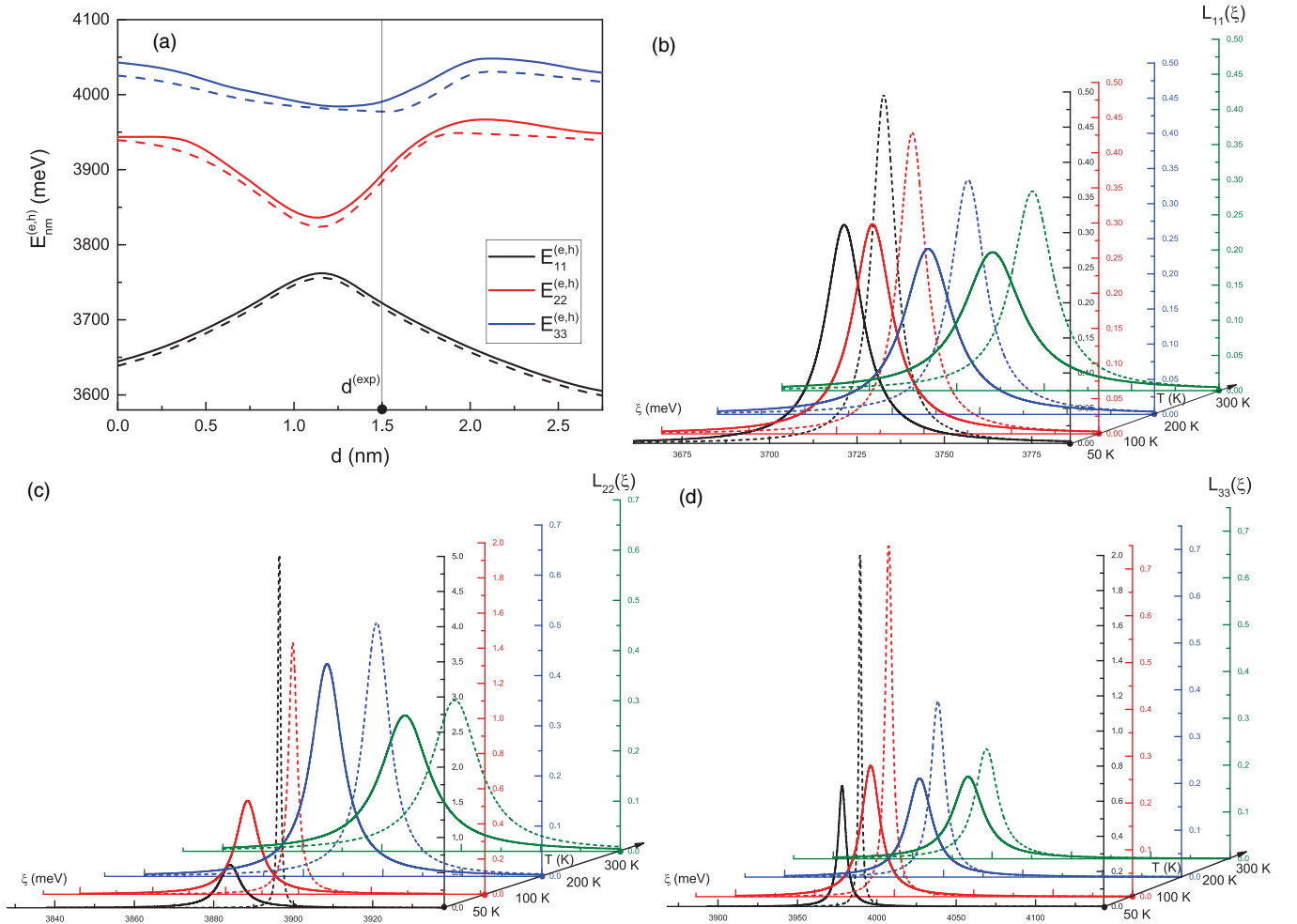


FIG. 7. The energies of electron-hole transitions $E_{nm}^{(e,h)}$ as functions of d (a) and exciton basic band shape functions (b)–(d), calculated in the vicinity of these energies for various temperatures. Solid lines correspond to wurtzite semiconductors and dashed lines correspond to zinc-blende semiconductors.

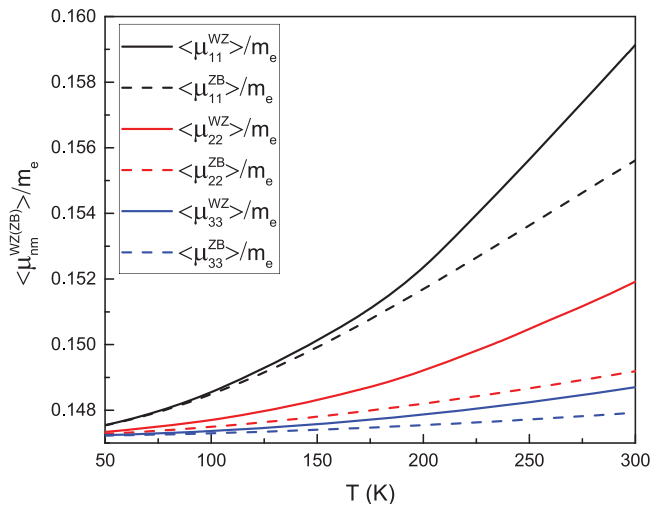


FIG. 8. Temperature dependencies of the effective exciton mass $\langle \mu_{nm} \rangle$ in the case when layers of nanosystem are of wurtzite semiconductors (solid lines) and zinc blende (dashed lines).

about 8% and 5%, respectively; for $\langle \mu_{11} \rangle$, for $\langle \mu_{22} \rangle$ and $\langle \mu_{33} \rangle$, these values are even less. Thus, it can be summarized that as the number of levels of electron and hole states increases, the effective mass of the exciton formed by these states is less and less renormalized due to interaction with acoustic phonons.

VI. SUMMARY

Summing up, it should be noted that the following main statements of the developed theory and results obtained on its basis were presented. A consistent analytical theory of the interaction of excitons with acoustic phonons in planar semiconductor nitride nanosystems have been developed. This theory takes into account both possible cases of orientation of the crystal lattice of nitride semiconductor nanosystems, the wurtzite type and zinc-blende type, respectively, and can be applied for arbitrary nonzero temperatures. First, using the model of effective masses for an electron and a hole, the exciton states were investigated and the exciton Hamiltonian was obtained in the representation of the second quantization. The theory is qualitatively specified by the use of exact analytical

expressions for the phonon modes obtained in the elastic continuum model, which determines its flexibility and variability and also makes it possible to be presented in the secondary quantization image of Hamiltonians, which are responsible for the interaction mechanisms through the deformation and piezoelectric potentials. Having performed the calculation of mass operators and applying the method of temperature Green's functions together with the Dyson equation, the problem of renormalizing the exciton spectrum was solved to obtain the characteristics of this spectrum: temperature shifts and decay rates. In addition, expressions were obtained for the exciton basic band-shape function and the renormalized exciton effective mass averaged over the nanosystem layers. Having performed calculations using the proposed theory, the following results were obtained.

We have found that for the energy levels of electrons and holes and the energies of electron-hole transitions in the case of a wurtzite nanosystem, their values somewhat prevail in the case of a zinc-blende nanosystem.

We have found that the deformation and piezoelectric potentials are of negative sign, but in the case of a wurtzite nanosystem these potentials are of the same order of magnitude, while for a zinc-blende nanosystem the deformation potential significantly exceeds the piezoelectric potential, being in this case the predominant factor contributing to the exciton-phonon interaction.

We have shown that the temperature shifts of the exciton spectrum calculated depending on the geometric configuration

of nanosystems have a negative sign, and the absolute values of the shifts have a clear tendency to increase with temperature increase. Similarly, we have established the temperature increase in the decay rates of the exciton states. We also found that the values of temperature shifts and decay rates for the same exciton states in the case of a wurtzite nanosystem are dominated by the same values for the zinc-blende nanosystem.

By analyzing the function of the absorption band calculated for temperatures from 50 K to 300 K, it was found that the effect of acoustic phonons suppresses electron-hole transitions, and this effect is much more sufficient for wurtzite nanosystems. In addition, for the half-width γ_{nm} in the case of zinc-blende nanosystems, we observe the effect that $\gamma_{22} \rightarrow 0$ and $\gamma_{33} \rightarrow 0$ if $T \rightarrow 0$ K.

We have found that the value of the renormalized exciton effective mass increases due to the interaction with acoustic phonons for all calculated temperatures, and the value of such an increase is up to 8% in the case of a wurtzite nanosystem and up to 5% in the case of a zinc-blende nanosystem. In this case, the temperature dependencies of the effective exciton mass are at first quasiquadratic, and at temperatures above 200 K they are quasilinear.

We hope that the proposed theory and results of calculation on its basis will be helpful for researchers working both in the field of theoretical and experimental investigation of the interaction of quasiparticles in nanosystems and in the field of optoelectronic devices such as QCLs and QCDs.

APPENDIX: ACOUSTIC PHONON MODES, CALCULATIONS OF PIEZOELECTRIC POTENTIAL

The solutions of Eq. (43) are as follows:

$$\begin{aligned} \phi_{pz}^{ZB}(z) &= A^{(p)} e^{qz} + B^{(p)} e^{-qz} - \frac{e_{14}^{(p)}}{\varepsilon_0 \varepsilon^{(p)} q} \sqrt{\frac{2\hbar}{S_{\perp} \rho^{(p)} \omega_{n_1 q}}} \left\{ e^{qz} \int_0^z e^{-q\xi} \Phi^{(p)}(q, \xi) d\xi - e^{-qz} \int_0^z e^{q\xi} \Phi^{(p)}(q, \xi) d\xi \right\}; \\ \Phi_s^{(p)}(q, \xi) &= q_x q_y w_3^{(p)}(z) - i \left(q_y \frac{dw_1^{(p)}(z)}{dz} + q_x \frac{dw_2^{(p)}(z)}{dz} \right) \\ &= -\frac{\sqrt{\rho^{(p)}} q_y}{\|u_s^{(p)}(q)\|} \sum_{s=1}^2 \left[q c_1^{(p)} \lambda_s^{(p)} + q_x \left\{ (\lambda_s^{(p)})^2 + (\chi_1^{(p)})^2 \right\} \right] \left(A_{2s-1}^{(p)} e^{\lambda_s^{(p)} z} + A_{2s}^{(p)} e^{-\lambda_s^{(p)} z} \right) + i q_x \chi \left(A_2^{(p)} e^{-\chi z} - B_2^{(p)} e^{\chi z} \right). \end{aligned} \quad (A1)$$

Acoustic phonon modes in the case of wurtzite semiconductors, which are solutions of Eq. (30), are as follows:

$$\begin{aligned} \tilde{u}_1^{(p)}(z) &= -i q c_1^{(p)} \sum_{s=1}^2 \left(\tilde{A}_{2s-1}^{(p)} e^{\lambda_s^{(p)} z} - \tilde{A}_{2s}^{(p)} e^{-\lambda_s^{(p)} z} \right) / \|u_s^{(p)}(q)\|, \\ \tilde{u}_3^{(p)}(z) &= -\sum_{s=1}^2 \left\{ (\lambda_s^{(p)})^2 + (\chi_1^{(p)})^2 \right\} \left(\tilde{A}_{2s-1}^{(p)} e^{\lambda_s^{(p)} z} + \tilde{A}_{2s}^{(p)} e^{-\lambda_s^{(p)} z} \right) / \|u_s^{(p)}(q)\|, \\ \| \tilde{u}_s^{(p)}(q) \| &= \sqrt{|q c_1^{(p)} \lambda_s^{(p)}|^2 + \left| (\lambda_s^{(p)})^2 + (\chi_1^{(p)})^2 \right|^2}, \quad \tilde{u}_2^{(p)}(z) = \tilde{A}_2^{(p)} e^{-\tilde{\chi} z} + \tilde{B}_2^{(p)} e^{\tilde{\chi} z}, \quad \tilde{\chi} = \sqrt{q^2 \frac{C_{66}^{(p)}}{C_{44}^{(p)}} - \frac{\rho^{(p)} \omega^2}{C_{44}^{(p)}}}. \end{aligned} \quad (A2)$$

Solutions of Eq. (50) look like the following:

$$\begin{aligned}
\phi_{\text{pz}}^{\text{WZ}}(z) &= \tilde{A}^{(p)} e^{qz} + \tilde{B}^{(p)} e^{-qz} - \frac{1}{\varepsilon_0 \varepsilon^{(p)}} \sqrt{\frac{\hbar}{2S_{\perp} \rho^{(p)} \omega_{n,q}}} \left\{ e^{qz} \int_0^z e^{-q\xi} \tilde{\Phi}_s^{(p)}(q, \xi) d\xi - e^{-qz} \int_0^z e^{q\xi} \tilde{\Phi}_s^{(p)}(q, \xi) d\xi \right\}; \\
\tilde{\Phi}_s^{(p)}(q, \xi) &= i(e_{15}^{(p)} + e_{31}^{(p)}) \left(q_x \frac{d\tilde{u}_1^{(p)}(z)}{dz} + q_y \frac{d\tilde{u}_2^{(p)}(z)}{dz} \right) + e_{15}^{(p)} q^2 \tilde{u}_3^{(p)}(z) - e_{31}^{(p)} \frac{d^2 \tilde{u}_3^{(p)}(z)}{dz^2} \\
&= \sqrt{\rho^{(p)}} \{ i(e_{15}^{(p)} + e_{31}^{(p)}) q_y \tilde{\chi} (\tilde{A}_2^{(p)} e^{-\tilde{\chi} z} - \tilde{B}_2^{(p)} e^{\tilde{\chi} z}) \\
&\quad + \sum_{s=1}^2 \{ (e_{15}^{(p)} + e_{31}^{(p)}) q c_1^{(p)} q_x \lambda_s^{(p)} - [e_{15}^{(p)} q^2 + e_{31}^{(p)} (\lambda_s^{(p)})^2] [(\lambda_s^{(p)})^2 + (\chi_1^{(p)})^2] \} \\
&\quad \times (\tilde{A}_{2s-1}^{(p)} e^{\lambda_s^{(p)} z} + \tilde{A}_{2s}^{(p)} e^{-\lambda_s^{(p)} z}) / \|u_s^{(p)}(q)\|. \tag{A3}
\end{aligned}$$

-
- [1] S. Chin, V. Mitev, E. Giraud, R. Maulini, S. Blaser, and D. L. Boiko, Electrically driven frequency blue-chirped emission in Fabry–Perot cavity quantum cascade laser at room temperature, *Appl. Phys. Lett.* **118**, 021108 (2021).
- [2] K. Wang, T. Grange, T. Lin, L. Wang, Z. Jehn, S. Birner, J. Yun, W. Terashima, and H. Hirayama, Broadening mechanisms and self-consistent gain calculations for GaN quantum cascade laser structures, *Appl. Phys. Lett.* **113**, 061109 (2018).
- [3] P. Quach, A. Jollivet, A. Babichev, N. Isac, M. Morassi, A. Lemaitre, P. A. Yunin, E. Frayssinet, P. de Mierry, M. Jeannin, A. Bousseksou, R. Colombelli, M. Tchernycheva, Y. Cordier, and F. H. Julien, A 5.7 THz GaN/AlGaIn quantum cascade detector based on polar step quantum wells, *Appl. Phys. Lett.* **120**, 171103 (2022).
- [4] P. M. Mensz, B. Dror, A. Ajay, C. Bougerol, E. Monroy, M. Orenstein, and G. Bahir, Design and implementation of bound-to-quasibound GaN/AlGaIn photovoltaic quantum well infrared photodetectors operating in the short wavelength infrared range at room temperature, *J. Appl. Phys.* **125**, 174505 (2018).
- [5] J. Gleize, M. A. Renucci, J. Frandon, and F. Demangeot, Anisotropy effects on polar optical phonons in wurtzite GaN/AlN superlattices, *Phys. Rev. B* **60**, 15985 (1999).
- [6] J.-j. Shi, Interface optical-phonon modes and electron–interface-phonon interactions in wurtzite GaN/AlN quantum wells, *Phys. Rev. B* **68**, 165335 (2003).
- [7] L. Li, D. Liu, and J.-J. Shi, Electron quasi-confined-optical-phonon interactions in wurtzite GaN/AlN quantum wells, *Eur. Phys. J. B* **44**, 401 (2005).
- [8] J. T. Lü and C. J. C, Confined optical phonon modes and electron-phonon interactions in GaN/ZnO wurtzite quantum wells, *Phys. Rev. B* **71**, 155304 (2005).
- [9] A. Cros and F. Pomer, Phonon dispersion in GaN/AlN non-polar quantum wells: Confinement and anisotropy, *Phys. Status Solidi C* **4**, 2515 (2007).
- [10] L. Zhang, Full optical phonon states and their dispersive spectra of a wurtzite GaN/AlGaIn superlattice: Quantum size effect, *Phys. Status Solidi B* **248**, 2120 (2011).
- [11] W. D. Huang, Y. J. Ren, J. F. Yan, Q. Wu, and S. H. Zhang, Propagating optical phonons and their properties in GaN/AlN quantum wells, *Eur. Phys. J. Appl. Phys.* **54**, 11301 (2011).
- [12] F. Q. Zhao and M. Zhang, Bound polarons in wurtzite GaN/AlGaIn quantum well, *Phys. Status Solidi C* **8**, 62 (2011).
- [13] W. D. Huang, Y. J. Ren, C. X. Xia, and S. Y. Wei, Dispersions of propagating optical phonons and electron-phonon interactions in wurtzite GaN/ZnO quantum wells, *Eur. Phys. J. Appl. Phys.* **57**, 11301 (2012).
- [14] Y. Qu and S. L. Ban, Electron mobility in wurtzite nitride quantum wells limited by optical-phonons and its pressure effect, *Eur. Phys. J. B* **69**, 321 (2009).
- [15] J. Zhu, B. S. L., and S. H. Ha, Phonon and electron-hole plasma effects on binding energies of excitons in wurtzite GaN/InGaIn quantum wells, *Eur. Phys. J. B* **85**, 67 (2012).
- [16] K. Park, A. Mohamed, M. Dutta, M. A. Stroschio, and C. Bayram, Electron scattering via interface optical phonons with high group velocity in wurtzite GaN-based quantum well heterostructure, *Sci. Rep.* **8**, 15947 (2018).
- [17] X. Zhou, Z. Wang, Y. Qu, and S. Ban, Electron mobility influenced by optical phonons in AlGaIn/GaN MISHEMTs with different gate dielectrics, *Appl. Phys. A* **126**, 825 (2020).
- [18] E. P. Pokatilov, D. L. Nika, and A. A. Balandin, Phonon spectrum and group velocities in AlN/GaN/AlN and related heterostructures, *Superlattices Microstruct.* **33**, 155 (2003).
- [19] E. P. Pokatilov, D. L. Nika, and A. A. Balandin, Confined electron-confined phonon scattering rates in wurtzite AlN/GaN/AlN heterostructures, *J. Appl. Phys.* **95**, 5626 (2004).
- [20] E. P. Pokatilov, D. L. Nika, A. S. Askerov, and A. A. Balandin, Size-quantized oscillations of the electron mobility limited by the optical and confined acoustic phonons in the nanoscale heterostructures, *J. Appl. Phys.* **102**, 054304 (2007).
- [21] Y. H. Zan, S. L. Ban, Y. J. Chai, and Y. Qu, Acoustic phonon modes in asymmetric AlGaIn/GaN/AlGaIn quantum wells, *Superlattices Microstruct.* **102**, 64 (2017).
- [22] I. Boyko, M. Petryk, and J. Fraissard, Spectrum and normalized modes of acoustic phonons in multilayer nitride-based nanostructure, *Eur. Phys. J. B* **93**, 57 (2017).

- [23] A. Balandin and K. L. Wang, Significant decrease of the lattice thermal conductivity due to phonon confinement in a free-standing semiconductor quantum well, *Phys. Rev. B* **58**, 1544 (1998).
- [24] J. Wang, L. Zhu, and W. Yin, Effects of heterogeneity and pre-stress field on phonon properties of semiconductor nanofilms, *Comput. Mater. Sci.* **145**, 14 (2018).
- [25] L. Zhu and H. Luo, Phonon properties and thermal conductivity of textscGaN nanofilm under prestress and surface/interface stress, *J. Alloys Compd.* **685**, 619 (2016).
- [26] L. Huang, S. Fan, L. Sang, Y. Mei, L. Ying, B. Zhang, and H. Long, Thermal conductivity and phonon scattering of AlGa_N nanofilms by elastic theory and Boltzmann transport equation, *Semicond. Sci. Technol.* **37**, 055003 (2016).
- [27] M. Smith, J. Y. Lin, H. X. Jiang, A. Khan, Q. Chen, A. Salvador, A. Botchkarev, W. Kim, and H. Morkoc, Exciton-phonon interaction in InGa_N/Ga_N and Ga_N/AlGa_N multiple quantum wells, *Appl. Phys. Lett.* **70**, 2882 (1997).
- [28] A. K. Viswanath, J. I. Lee, D. Kim, C. R. Lee, and J. Y. Leem, Exciton-phonon interactions, exciton binding energy, and their importance in the realization of room-temperature semiconductor lasers based on Ga_N, *Phys. Rev. B* **58**, 16333 (1998).
- [29] S. J. Xu, L. X. Zheng, S. H. Cheung, M. H. Xie, and S. Y. Tong, Comparative study on the broadening of exciton luminescence linewidth due to phonon in zinc-blende and wurtzite Ga_N epilayers, *Appl. Phys. Lett.* **81**, 4389 (2002).
- [30] I. A. Ostapenko, G. Hönig, S. Rodt, A. Schliwa, A. Hoffmann, D. Bimberg, M.-R. Dachner, M. Richter, A. Knorr, S. Kako, and Y. Arakawa, Exciton acoustic-phonon coupling in single Ga_N/Al_N quantum dots, *Phys. Rev. B* **85**, 081303(R) (2012).
- [31] M. Bouzidi, S. Soltani, I. Halidou, Z. Chine, and B. El Jani, Photoreflectance investigation of exciton-acoustic phonon scattering in Ga_N grown by Ga_N grown by MOVPE, *Solid State Sci.* **54**, 59 (2016).
- [32] N. Grigorukh, Exciton-phonon coupling functions in uniaxial crystals, *Phys. Rev. B* **55**, 888 (1997).
- [33] N. I. Grigorukh, Exciton-phonon coupling and exciton damping due to acoustic phonons in anisotropic nonpolar crystals, *J. Phys.: Condens. Matter* **11**, 417 (1999).
- [34] A. Sedhain, J. Li, J. Y. Lin, and H. X. Jiang, Probing exciton-phonon interaction in Al_N epilayers by photoluminescence, *Appl. Phys. Lett.* **95**, 061106 (2009).
- [35] I. A. Aija, P. R. Edwards, Z. Liu, J. C. Yan, R. W. Martin, and I. S. Roqan, Excitonic localization in Al_N-rich multi-quantum-well grain boundaries, *Appl. Phys. Lett.* **105**, 122111 (2014).
- [36] D. Bayerl and E. Kioupakis, Room-temperature stability of excitons and transverse-electric polarized deep-ultraviolet luminescence in atomically thin Ga_N quantum wells, *Appl. Phys. Lett.* **115**, 131101 (2019).
- [37] G. Staszczak, W. Trzeciakowski, E. Monroy, A. Bercha, G. Muzioł, C. Skierbiszewski, P. Perlin, and T. Suski, Hydrostatic pressure dependence of indirect and direct excitons in InGa_N/Ga_N quantum wells, *Phys. Rev. B* **101**, 085306 (2020).
- [38] I. Vurgaftman and J. R. Meyer, Band parameters for nitrogen-containing semiconductors, *J. Appl. Phys.* **94**, 3675 (2003).
- [39] F. Bernardini, V. Fiorentini, and D. Vanderbilt, Spontaneous polarization and piezoelectric constants of III-V nitrides, *Phys. Rev. B* **56**, R10024(R) (1997).
- [40] F. Bernardini and V. Fiorentini, Macroscopic polarization and band offsets at nitride heterojunctions, *Phys. Rev. B* **57**, R9427(R) (1998).
- [41] F. Bernardini and V. Fiorentini, Spontaneous versus piezoelectric polarization in III-V nitrides: Conceptual aspects and practical consequences, *Phys. Status Solidi B* **216**, 391 (1999).
- [42] A. Zoroddu, F. Bernardini, P. Ruggerone, and V. Fiorentini, First-principles prediction of structure, energetics, formation enthalpy, elastic constants, polarization, and piezoelectric constants of Al_N, Ga_N, and In_N: Comparison of local and gradient-corrected density-functional theory, *Phys. Rev. B* **64**, 045208 (2001).
- [43] A. D. Polyani and V. F. Zaitsev, *Handbook of Ordinary Differential Equations Exact Solutions, Methods, and Problems* (CRC Press, Boca Raton, New York, London, 1995).
- [44] H. Wang, G. A. Farias, and V. N. Freire, Interface-related exciton-energy blueshift in Ga_N/AlGa_N zinc-blende and wurtzite single quantum wells, *Phys. Rev. B* **60**, 5705 (1999).
- [45] J. Zhu, S. L. Ban, and S. H. Ha, Binding energies of excitons in strained [0001]-oriented wurtzite AlGa_N/Ga_N double quantum wells, *Phys. Status Solidi B* **248**, 384 (1999).
- [46] I. V. Boyko, M. R. Petryk, and J. Fraissard, Theory of the shear acoustic phonons spectrum and their interaction with electrons due to the piezoelectric potential in Al_N/Ga_N nanostructures of plane symmetry, *Low Temp. Phys.* **47**, 141 (2021).
- [47] I. V. Boyko, M. R. Petryk, and J. Fraissard, Investigation of the electron-acoustic phonon interaction via the deformation and piezoelectric potentials in Al_N/Ga_N resonant tunneling nanostructures, *Superlattices Microstruct.* **156**, 106928 (2021).
- [48] R. S. Knox, *Theory of Excitons* (Academic Press, New York, 1963).
- [49] I. Vurgaftman, J. R. Meyer, and L. R. Ram-Mohan, Band parameters for III-V compound semiconductors and their alloys, *J. Appl. Phys.* **89**, 5815 (2001).
- [50] A. E. Romanov, T. J. Baker, S. Nakamura, and J. S. Speck, Strain-induced polarization in wurtzite III-nitride semipolar layers, *J. Appl. Phys.* **100**, 023522 (2006).
- [51] S. Sakr, E. Giraud, M. Tchernycheva, N. Isac, P. Quach, E. Warde, N. Grandjean, and F. H. Julien, A simplified Ga_N/AlGa_N quantum cascade detector with an alloy extractor, *Appl. Phys. Lett.* **101**, 251101 (2012).
- [52] S. Sakr, E. Giraud, A. Dussaigne, M. Tchernycheva, N. Grandjean, and F. H. Julien, Two-color Ga_N/AlGa_N quantum cascade detector at short infrared wavelengths of 1 and 1.7 μm, *Appl. Phys. Lett.* **100**, 181103 (2012).
- [53] X. Gao, D. Botez, and I. Knezevic, X-valley leakage in GaAs-based midinfrared quantum cascade lasers: A Monte Carlo study, *J. Appl. Phys.* **101**, 063101 (2007).
- [54] N. Bannov, V. Mitin, and M. Stroschio, Confined acoustic phonons in a free-standing quantum well and their interaction with electrons, *Phys. Status Solidi B* **183**, 131 (1994).